Supplementary Information

Redox-controlled chalcogen-bonding at tellurium: Impact on Lewis acidity and chloride anion transport properties

Benyu Zhou and François P. Gabbaï

Department of Chemistry, Texas A&M University, College Station, Texas 77843-3255, United States of America

Contents

1 Synthesis and characterization

1.1 General considerations

The syntheses were carried out in a well-ventilated fumehood with proper shielding to mitigate hazards associated to the use of pyrophoric reagents, potentially explosive metallated fluorinated compounds, and potentially toxic organotellurium derivatives. All commercially available materials including tellurium powder, magnesium powder, mesityl bromide, pentafluorophenyl bromide, methyl iodide, silver tetrafluoroborate, and trimethyl oxonium tetrafluoroborate salt were used without further purification. Egg yolk phosphatidylcholine (EYPC) was purchased from Avanti Polar Lipids. Valinomycine was purchased from BioWorld, potassium gluconate from TCI America. The Sephadex G-50 column was purchased from GE Healthcare – Life Sciences. Solvents were dried by refluxing over Na/K (Et_2O, THF), K (toluene), or CaH_2 (CH_2Cl_2). All other solvents were ACS reagent grade and used as received. The syntheses of the tellurides and that of bis(pentafluorophenyl) methyl telluronium tetrafluoroborate were carried out under a dry N_2 atmosphere with standard Schlenk techniques. NMR spectra were recorded at room temperature using a Varian Inova 500 FT NMR (499.41 MHz for ^1H) spectrometer, a Bruker Avance 500 NMR spectrometer, or a Bruker Ascend 400 NMR spectrometer. Chemical shifts are given in ppm.^1H and ^{13}C signals were referenced to residual ^1H or ^{13}C solvent signals. The ^{19}F signals are referenced using C_6F_6 as a secondary external standard set at -161.64 ppm *vs.* $CFCl_3$.[1] The ^{125}Te signals were referenced using Ph_2Te_2 as a secondary standard set at 422.0 ppm *vs.* Me_2Te.[2] All ^{125}Te NMR spectra were recorded in the presence of a sealed capillary containing a $CDCl_3$ solution of Ph_2Te_2. Elemental analyses were performed by Atlantic Microlab (Norcross, GA). ISE assays were performed with an Oakton WD-35812-12 Chloride Double-junction Economy Epoxy Ion Selective Electrode connected to a pH-meter giving readings in mV (PHM 290, Meter lab, Radiometer Analytical S.A., Villeurbanne, Cedex, France).

1.2 Synthetic procedures

Dimesityl ditelluride

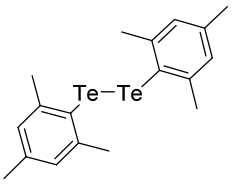

The synthesis of dimesityl ditelluride was adapted from literature procedures.[3, 4] 2-Bromomesitylene (15 mL, 19.8 g, 99.6 mmol) was added dropwise over the course of 1h to a gently refluxing suspension of magnesium powder (2.66 g, 110 mmol) in anhydrous THF (50 mL). Upon completion of the addition, the solution was stirred for another 1 h. The freshly-made mesityl Grignard solution was cooled to r.t. and transferred to another Schlenk flask containing Te powder (12.7 g, 99.6 mmol). The resulting black suspension was stirred overnight at r.t. then exposed to air with stirring for 2 h. After removal of all volatiles under reduced pressure, the residue was extracted with Et_2O (50 mL × 3) and filtered. The filtrate was brought to dryness using a rotary evaporator, affording a dark red solid. This solid was treated with benzene (20 mL) and hexanes (60 mL) affording a solution that was filetered to remove insoluble impurities. Addition of EtOH 200 mL) to the filtrate resulted in the precipitation of the dimesityl ditelluride as a red crystalline solid (8.43 g, 34%). **^{1}H NMR** (400 MHz, $CDCl_3$) δ 6.89 (s, 4H, *m*-H), 2.39 (s, 12 H, *o*-Me), 2.34 (s, 6H, *p*-Me). **^{125}Te NMR** (126 MHz, $CDCl_3$) δ 196.0 (s). The chemical shifts are consistent with the literature values.[3, 4]

1: Dimesityl telluride

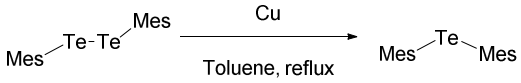

This compound was synthesized by following a published procedure.[3] The specific quantities and conditions used in our experiment are provided hereafter. A solution of Mes_2Te_2 (3.27 g, 6.63 mmol) in anhydrous toluene (40 mL) was refluxed overnight in the presence of copper powder (1.69 g, 26.5 mmol). The dark red suspension was cooled to r.t. then filtered. The light yellow filtrate was brought to dryness under reduced pressure affording the dimesityl telluride as an off-white solid (2.33 g, 96 %). **^{1}H NMR** (500 MHz, $CDCl_3$) δ 6.87 (s, 4H, *m*-H), 2.35 (s, 12H, *o*-Me), 2.25 (s, 6H, *p*-Me). **^{13}C NMR** (126 MHz, $CDCl_3$) δ 144.3 (s, $^{2}J_{125Te\text{-}13C}$ = 12.8Hz, Mes-*C*2), 138.0 (s, Mes-*C*4), 127.9 (s, Mes-*C*3), 117.2 (s & d, $^{1}J_{125Te\text{-}13C}$ = 295.3 Hz, Mes-*C*1), 28.2 (s, Mes-*o*-*Me*), 21.0 (s, Mes-*p*-*Me*). **^{125}Te NMR** (126 MHz, $CDCl_3$) δ 258.7 (s). The chemical shifts are consistent with the literature values.[3]

2: Pentafluorophenyl mesityl telluride

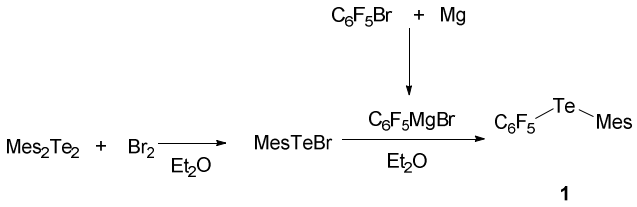

A solution of bromopentafluorobenzene (0.75 mL, 1.48 g, 6.0 mmol) in anhydrous Et_2O (2 mL) was added dropwise to a magnesium powder (181 mg, 7.4 mmol) suspended in anhydrous Et_2O (10 mL). The reaction was initiated by mild heating after a small portion of the aryl bromide was added. The rate of addition was such that the gentle refluxing was preserved throughout the addition of the aryl bromide. Upon completion of the addition, the solution was refluxed for 2 h and cooled to room temperature. In a separate flask, liquid bromine (0.2 mL, 3.9 mmol) was added to a solution of dimesityl ditelluride (1.63 g, 3.3 mmol) in Et_2O (20 mL) at 0°C leading to the formation of MesTeBr. Next, the Girgnard solution was slowly added to the freshly made solution of MesTeBr in Et_2O (20 mL) at 0°C. The mixture was allowed to warm to r.t. and stirred at this temperature for an additional 2 h. The mixture was neutralized by addition of a small amount of aqueous HCl. The organic phase was washed with a saturated NH_4Cl solution (40 mL). The aqueous phase was extracted with Et_2O (60 mL × 2) then the organic phases were combined and dried with anhydrous magnesium sulfate. After removal of all volatiles under reduced pressure, the crude product was extracted with Hexanes and filtered through a silica plug. The yellow filtrate was evaporated under reduced pressure affording a residue which was recrystallized in Hexanes. This procedure yielded pentafluorophenyl mesityl telluride **2** as a yellow powder (1.90 g, 76%). **^{1}H NMR** (500 MHz, $CDCl_3$) δ 6.98 (s, *m*-H), 2.59 (s, *o*-Me), 2.29 (s, *p*-Me). **^{13}C NMR** (126 MHz, $CDCl_3$) δ 147.9 (dm, $^1J_{19F\text{-}13C}$ = 241.0 Hz, C_6F_5-*C*2), 145.6 (s, Mes-*C*2), 141.7 (dm, $^1J_{19F\text{-}13C}$ = 254.5 Hz, C_6F_5-*C*4), 140.4 (s, Mes-*C*4), 136.9 (dm, $^1J_{19F\text{-}13C}$ = 254.0 Hz, C_6F_5-*C*4), 127.9 (s, Mes-*C*3), 116.8 (s & d, $^1J_{125Te\text{-}13C}$ = 272.9 Hz, Mes-*C*1), 87.20 (tm, $^2J_{19F\text{-}13C}$ = 32.0 Hz, C_6F_5-*C*1), 29.7 (s, Mes-*o*-*Me*), 21.09 (s, Mes-*p*-*Me*). **^{19}F NMR**(470 MHz, $CDCl_3$) δ -119.6 (m, 2F, *o*-F), -155.2 (m, 1F, *p*-F), -162.8 (m, 2F, *m*-F). **^{125}Te NMR**(126 MHz, $CDCl_3$) δ 280.0 (t, $^3J_{19F\text{-}125Te}$ = 49.1 Hz). **Elemental analysis** (%) calculated : C, 43.53; H, 2.68. Found: C, 43.48; H, 2.69.

3: Bis(pentafluorophenyl) telluride

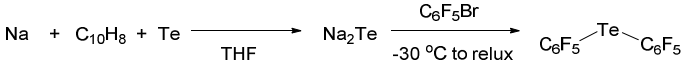

The synthesis of bis(pentafluorophenyl) telluride was adapted from literature procedures.[5, 6] Na (336 mg, 14.6 mmol) and naphthalene (1.87 g, 14.6 mmol) were suspended in anhydrous THF (30 mL) and stirred

for 1 h to afford a dark green sodium naphthalenide solution to which was added tellurium powder (931.5 mg, 7.3 mmol). The suspension was stirred overnight during which time the green color faded away, affording a grey suspension Na_2Te. This suspension was cooled to -30 °C and treated with a solution of bromopentafluorobenzene (1.9 mL in 10 ml anhydrous THF, 15.2 mmol) which was added dropwise, leading to an orange-red solution. The mixture was stirred at -30 °C for 1 h then heated to reflux for 18 h. The solution was cooled to r.t. and filtered using a frit. The solid residue left on the frit was washed with THF (5 mL × 3) in order to extract more product. The light orange filtrate was brought to dryness under reduced pressure, affording a yellow solid consisting mainly of the product and naphthalene. Purification was achieved using column chromatography (Hexanes). The product, which eluted after naphthalene, was obtained as a yellow crystalline powder (1.46 g, 43 %). NMR indicated a trace amount (less than 1%) of naphthalene leftover. **^{13}C-NMR** (126 MHz, $CDCl_3$) δ 147.9 (dm, $^1J_{19F\text{-}13C}$ = 243.4 Hz, C2), 143.2 (dm, $^1J_{19F\text{-}13C}$ = 257.3 Hz, C4), 137.1 (dm, $^1J_{19F\text{-}13C}$ = 255.3 Hz, C3), 85.0c (tm, $^2J_{19F\text{-}13C}$ = 31.2 Hz, C1). **^{19}F-NMR** (470 MHz, $CDCl_3$) δ -117.8 (m, 4F, *o*-F), -151.7 (m, 2F, *p*-F), -161.4 (m, 4F, *m*-F). **^{125}Te-NMR** (126 MHz, $CDCl_3$) δ 287.1 (quinquin, $^3J_{19F\text{-}125Te}$ = 49.8 Hz, $^3J_{19F\text{-}125Te}$ = 8.5 Hz). These chemical shifts are consistent with literature values.[5]

4: Dimesityl methyl telluronium tetrafluoroborate ([2][BF$_4$])

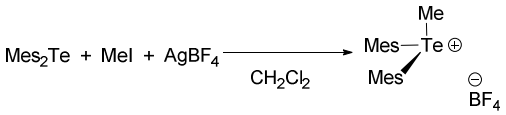

[**2**][BF_4]

Solid Mes_2Te (300 mg, 0.820 mmol) and $AgBF_4$ (160 mg, 0.820 mmol) were combined in anhydrous CH_2Cl_2 (5 mL) and treated with MeI (0.5 mL, 1.14 g, 8.03 mmol) which was added dropwise, affording an heterogenous solution. This solution was stirred overnight and filtered. The filtrate was brought to dryness affording a light yellow solid containing [**2**][BF_4]. The pure telluronium salt [**2**][BF_4] was obtained as a white solid (336 mg, 88%). by washing the crude product with Et_2O (5 mL × 3)**.** A single crystal was grown by vapor diffusion of Et_2O into a $CHCl_3$ solution of [**2**][BF_4]. **^{1}H NMR** (500 MHz, $CDCl_3$) δ 6.99 (s, 4H, *m*-H), 3.17 (s & d, $^2J_{125Te\text{-}1H}$ = 29.1 Hz, 3H, Te-*Me*), 2.36 (s, 12H, *o*-Me), 2.31 (s, 6H, *p*-Me). **^{13}C NMR** (126 MHz, $CDCl_3$) δ 143.3 (s, C4), 142.9 (s & d, $^2J_{125Te\text{-}13C}$ = 27.6 Hz, C2), 131.5 (s, C3), 118.7 (s & d, $^1J_{125Te\text{-}13C}$ = 254.2 Hz, C1), 11.9 (s & d, $^1J_{125Te\text{-}13C}$ = 177.1 Hz, Te-*Me*). **^{19}F NMR** (470 MHz, $CDCl_3$) δ -152.9 (m, BF_4^-);**^{125}Te NMR** (126 MHz, $CDCl_3$) δ 563.7 (s). **Elemental analysis** (%) calculated : C, 48.78; H, 5.39. Found: C, 48.98; H, 5.53.

5: Pentafluorophenyl mesityl methyl telluronium tetrafluoroborate ([3][BF_4])

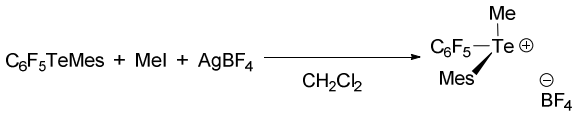

[**3**][BF_4]

Solid C_6F_5TeMes (300 mg, 0.725 mmol) and $AgBF_4$ (141 mg, 0.725 mmol) were combined in anhydrous CH_2Cl_2 (5 mL) and treated with MeI (0.5 mL, 1.14 g, 8.03 mmol) which was added dropwise, affording an heterogenous solution. This solution was stirred overnight and filtered. The filtrate was brought to dryness affording a light yellow solid containing [**3**][BF_4]. Recrystallization of the crude product from CH_2Cl_2/Et_2O afforded [**3**][BF_4] as a white powder (259 mg, 69%). A single crystal was grown by vapor diffusion of Et_2O into a $CHCl_3$ solution of [**3**][BF_4]. **^{1}H NMR** (500 MHz, $CDCl_3$) δ 7.03 (s, 2H, *m*-H), 3.45 (s & d, $^2J_{125Te\text{-}1H}$ = 31.2 Hz, 3H, Te-*Me*), 2.57 (s, 6H, *o*-Me), 2.32 (s, 3H, *p*-Me). **^{13}C NMR** (126 MHz, $CDCl_3$) δ 147.9 (dm, $^1J_{19F\text{-}13C}$ = 247.8 Hz, C_6F_5-*C*2), 144.4 (s, Mes-*C*4), 144.3 (dm, $^1J_{19F\text{-}13C}$ = 261.1 Hz, C_6F_5-*C*4), 144.0(s & d, $^2J_{125Te\text{-}13C}$ = 34.7 Hz, Mes-*C*2), 138.0 (dm, $^1J_{19F\text{-}13C}$ = 260.5 Hz, C_6F_5-*C*3), 131.4 (s, Mes-*C*3), 119.4 (s & d, $^1J_{125Te\text{-}13C}$ = 267.3 Hz, Mes-*C*1), 93.0(tm, $^2J_{19F\text{-}13C}$ = 26.2 Hz, C_6F_5-*C*1), 24.2 (s & d, $^2J_{125Te\text{-}13C}$ = 37.7 Hz, Mes-*o*-*Me*), 21.2 (s, Mes-*p*-*Me*), 10.6 (t, $^4J_{19F\text{-}13C}$ = 5.6 Hz, Te-*Me*). **^{19}F NMR** (470 MHz, $CDCl_3$) δ -127.3 (m, 2F, *o*-F), -147.1 (m, 1F, *p*-F), -149.8 (m, 4F, BF_4^-), -159.1 (m, 2F, *m*-F); **^{125}Te NMR** (126 MHz, $CDCl_3$) δ 637.4 (m). **Elemental analysis** (%) calculated : C, 37.27; H, 2.74. Found: C, 37.54; H, 2.68.

6: Bis(pentafluorophenyl) methyl telluronium tetrafluoroborate ([4][BF_4])

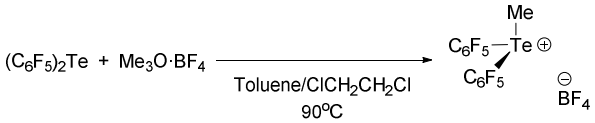

[**4**][BF_4]

Bis(pentafluorophenyl) telluride (300 mg, 0.650 mmol) and trimethyloxonium tetrafluoroborate (288 mg, 1.95 mmol) were suspended in a solution consisting of anhydrous toluene (4 mL) and anhydrous 1,2-dichloroethane (2 mL). The resulting suspension was heated to 90°C affording an homogeneous solution which was refluxed overnight. After cooling to r.t., the product that had precipitated overnight was isolated by filtration and washed with Et_2O (5 mL × 3), affording [**4**][BF_4] as a white powder (166 mg, 45%). A single crystal was obtained by vapor diffusion of Et_2O into a CH_3CN solution of [**4**][BF_4]. **^{1}H NMR** (500 MHz, CD_3CN) δ 3.44 (s & d, $^2J_{125Te\text{-}1H}$ = 31.0 Hz, Te-Me). **^{13}C NMR** (126 MHz, CD_3CN) δ 148.8 (dm, $^1J_{19F\text{-}13C}$ = 247.7 Hz, C2), 145.9 (dm, $^1J_{19F\text{-}13C}$ = 258.8 Hz, C4), 139.1 (dm, $^1J_{19F\text{-}13C}$ = 256.9 Hz, C3), 96.2

(tm, $^{2}J_{19F\text{-}13C}$ = 26.7 Hz, C1), 12.8 (quint & d, $^{4}J_{19F\text{-}13C}$ = 5.2 Hz, $^{1}J_{125Te\text{-}13C}$ = 159.4 Hz, Te-*Me*). **^{19}F NMR** (470 MHz, CD_3CN) δ -127.0 (m, 4F, *o*-F), -148.1 (m, 2F, *p*-F), -153.0 (m, 4F, BF_4^-), -160.9 (m, 4F, *m*-F). **^{125}Te NMR** (126 MHz, CD_3CN) δ 598.1 (m). **Elemental analysis** (%) calculated: C, 27.71; H, 0.54. Found: C, 27.76; H, 0.51.

1.3 NMR spectra

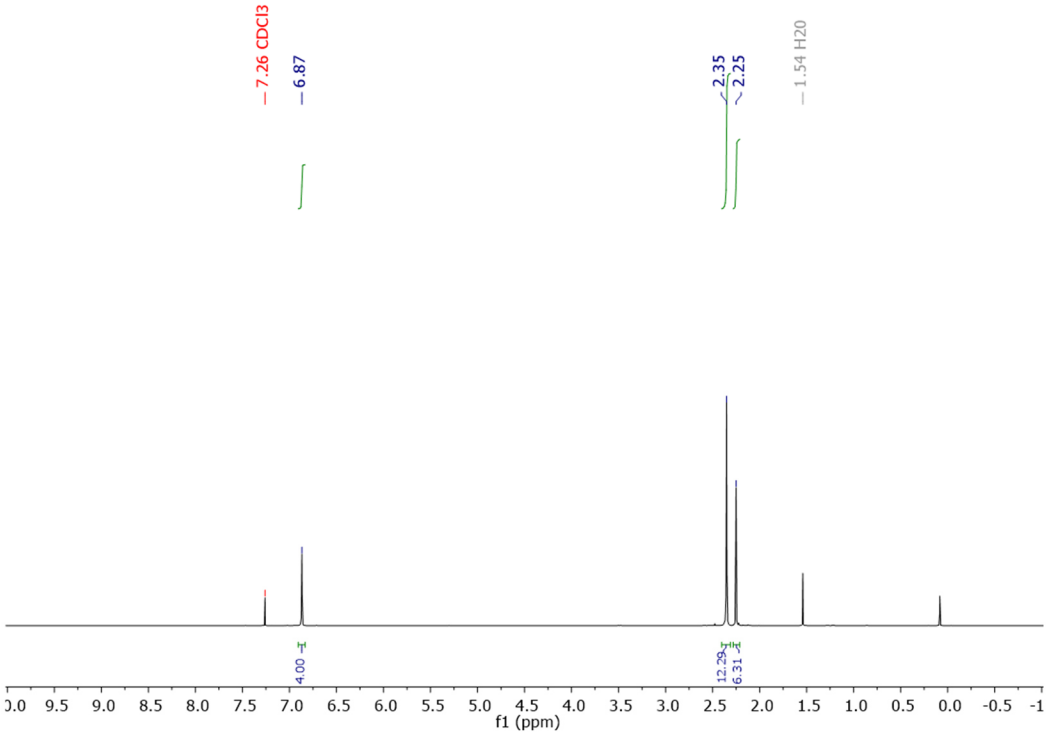

Figure S1. ^{1}H-NMR spectrum of Mes_2Te in $CDCl_3$.

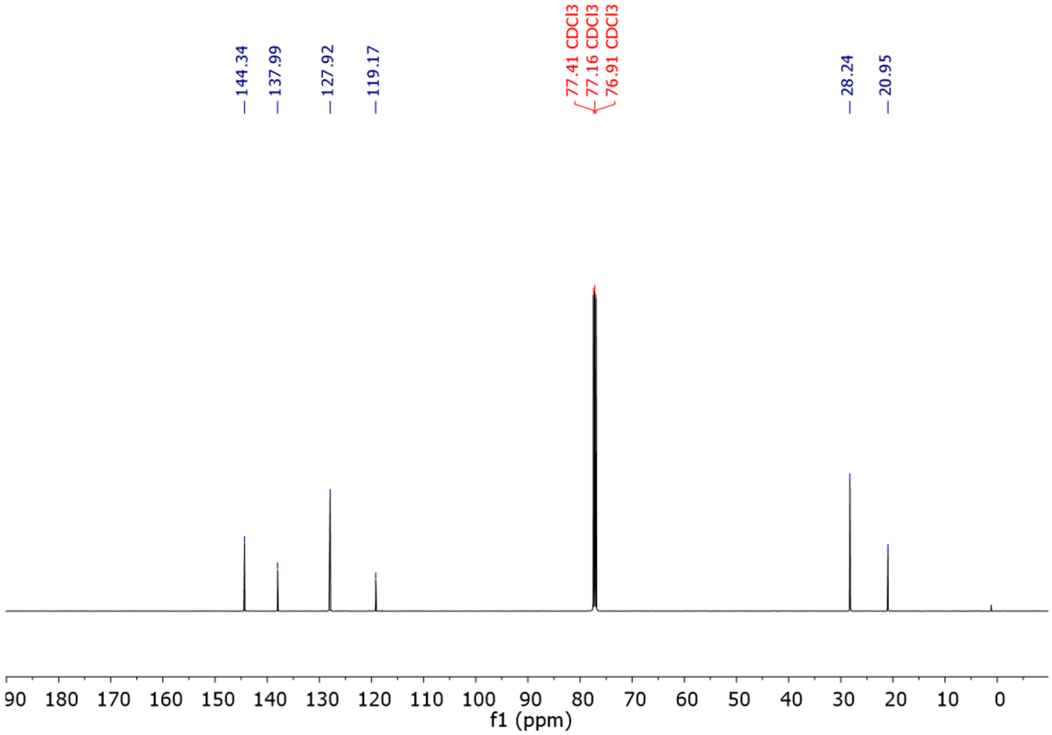

Figure S2. ^{13}C-NMR spectrum of Mes_2Te in $CDCl_3$.

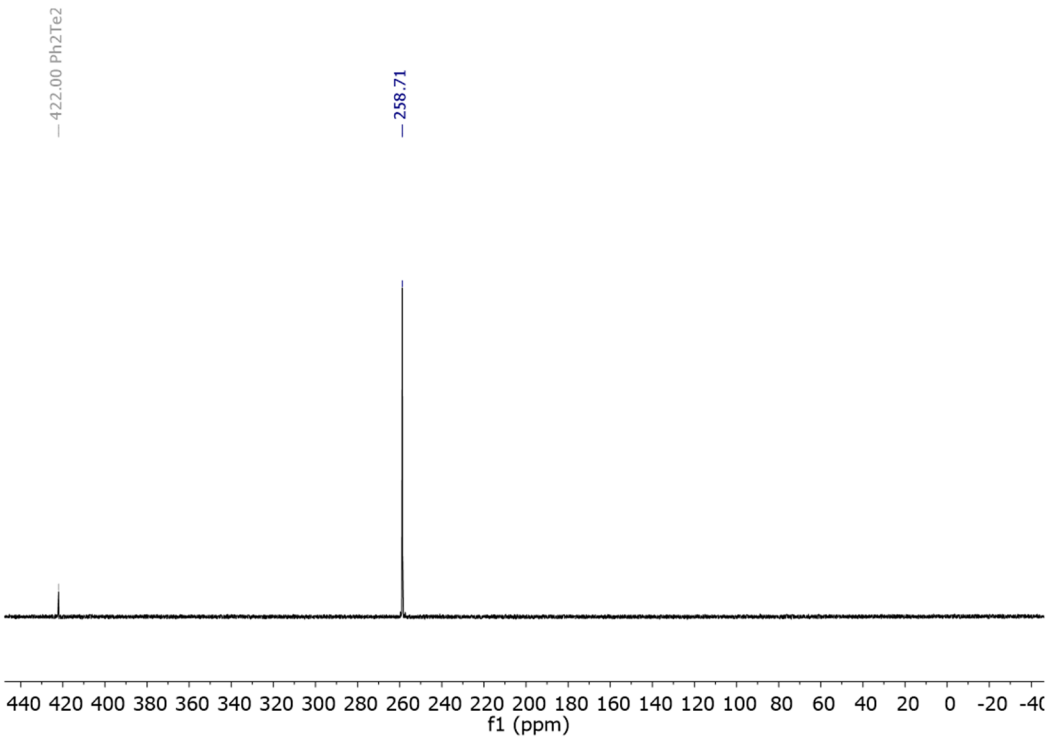

Figure S3. ^{125}Te-NMR spectrum of Mes_2Te in $CDCl_3$

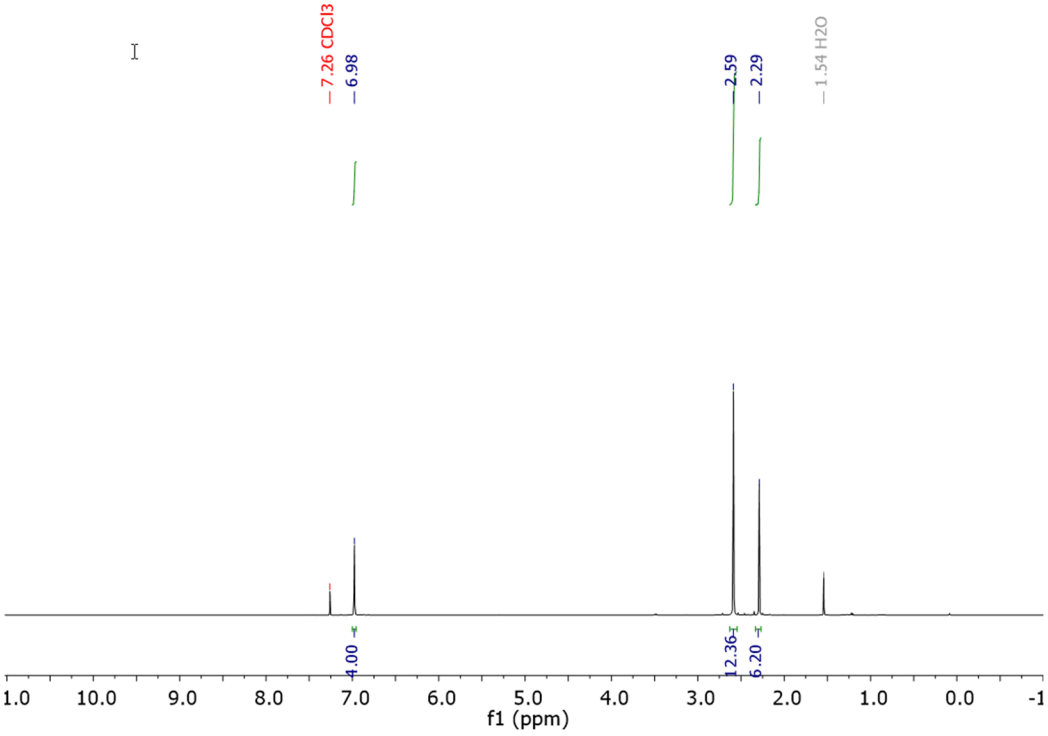

Figure S4. ^{1}H-NMR spectrum of $Mes(C_6F_5)Te$ (**1**) in $CDCl_3$.

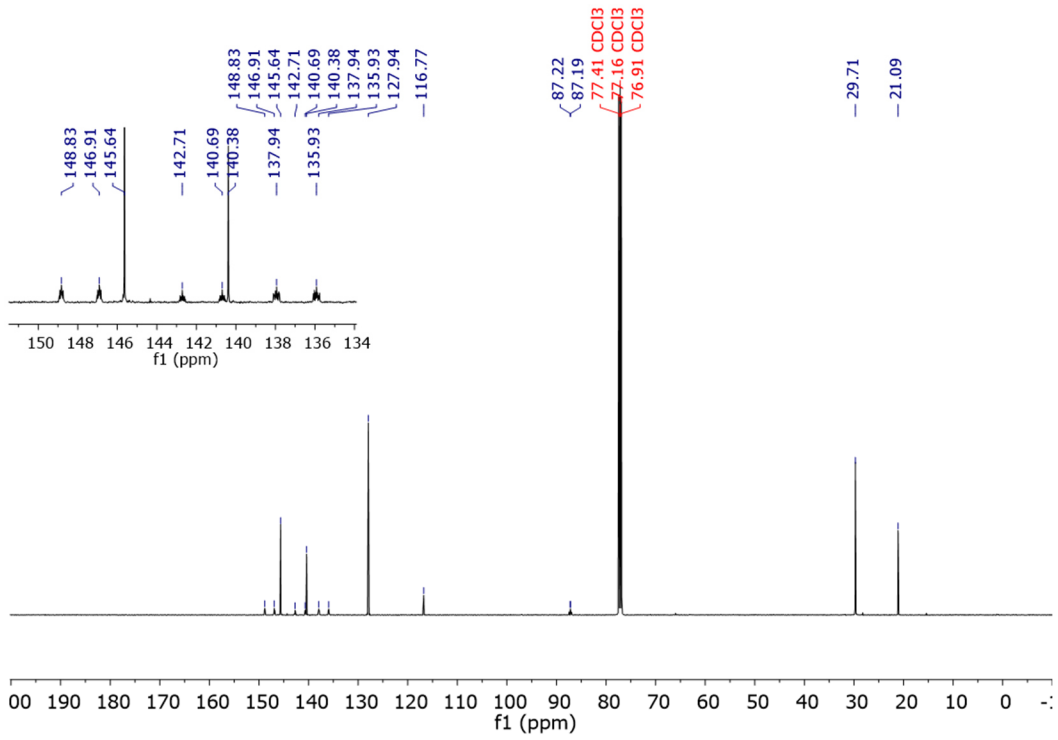

Figure S5. ^{13}C-NMR spectrum of Mes(C_6F_5)Te (**1**) in $CDCl_3$.

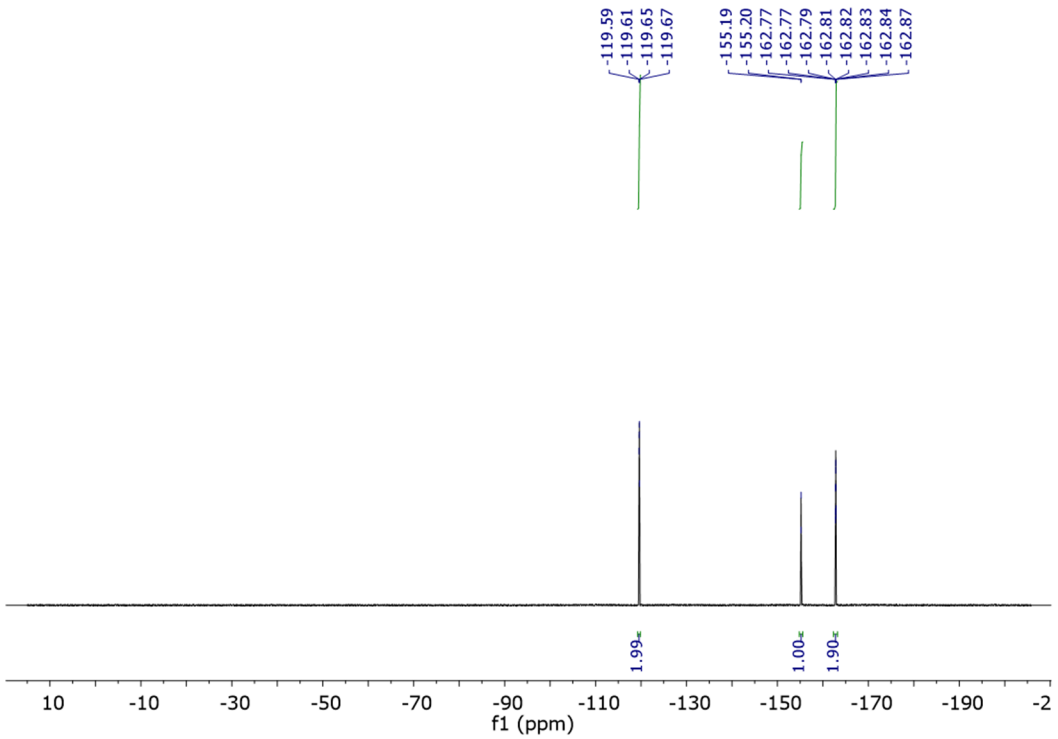

Figure S6. ^{19}F-NMR spectrum of Mes(C_6F_5)Te (**1**) in $CDCl_3$.

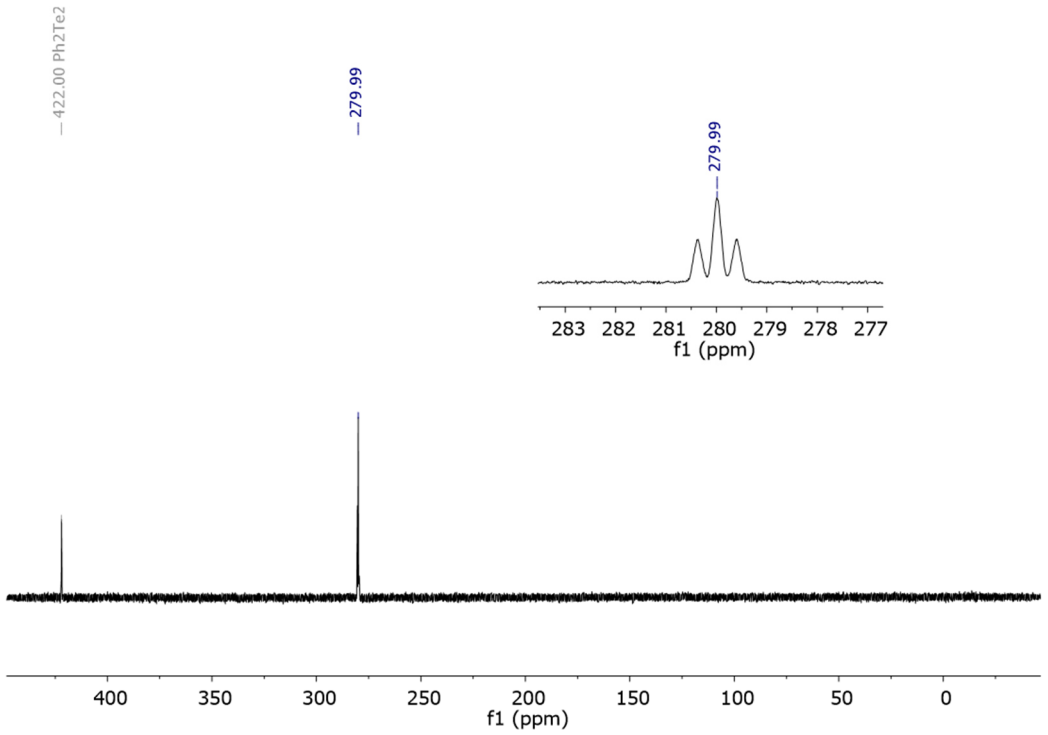

Figure S7. ^{125}Te-NMR spectrum of Mes(C_6F_5)Te (**1**) in $CDCl_3$.

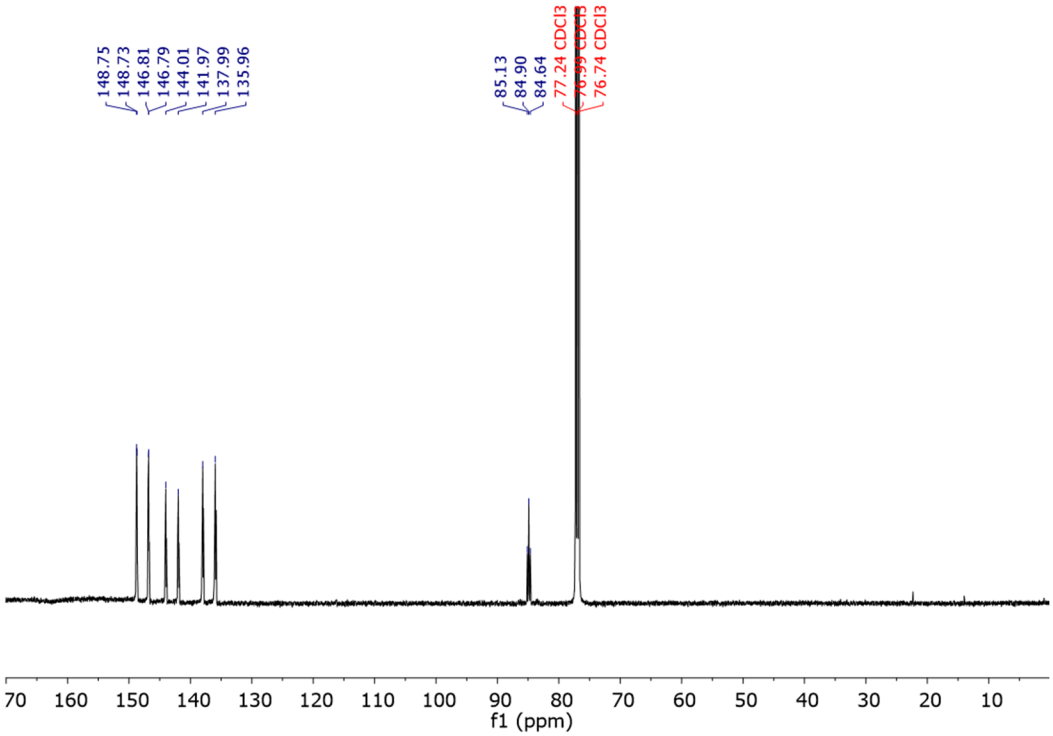

Figure S8. ^{13}C-NMR spectrum of $(C_6F_5)_2$Te in $CDCl_3$.

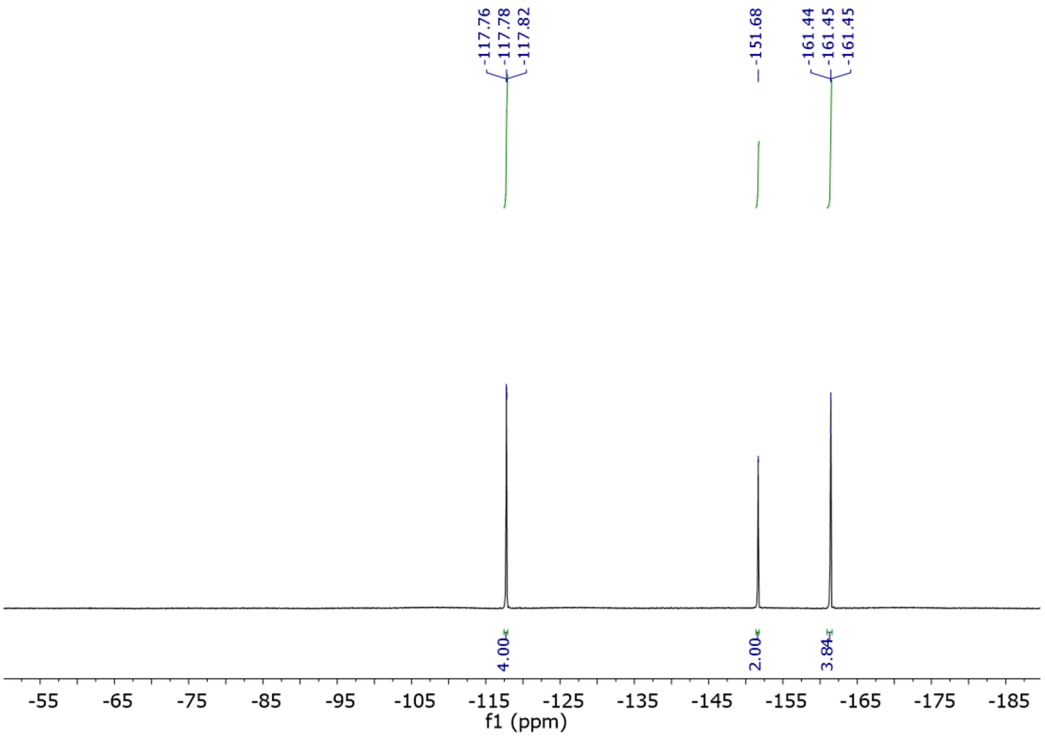

Figure S9. ^{19}F-NMR spectrum of $(C_6F_5)_2Te$ in $CDCl_3$.

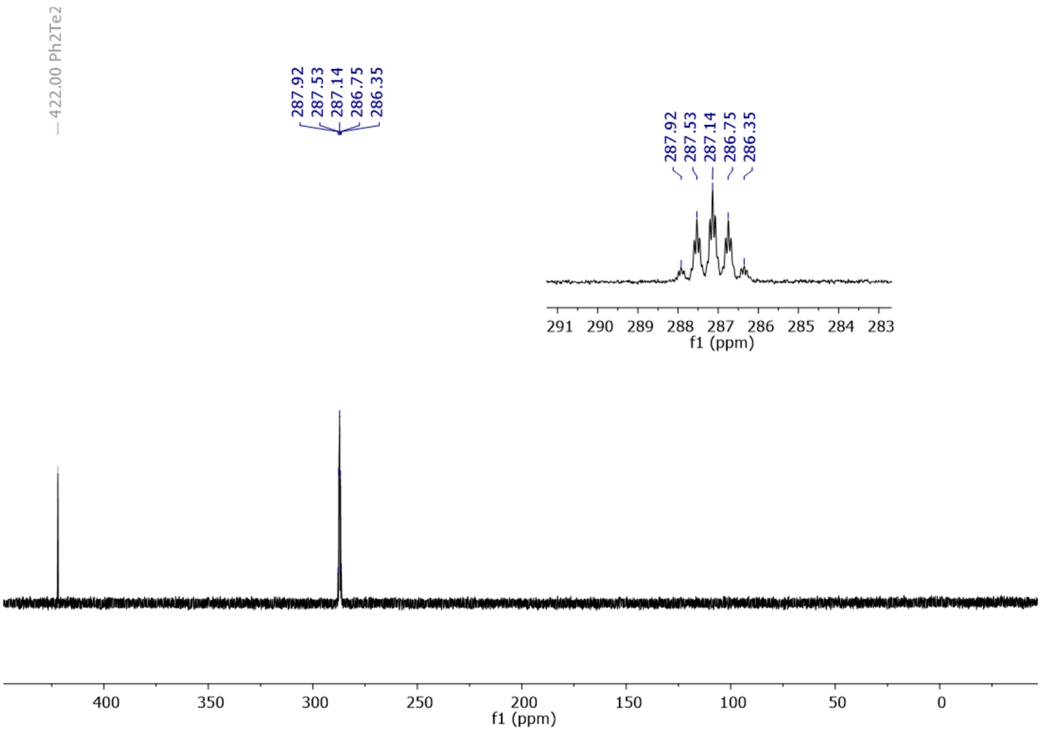

Figure S10. ^{125}Te-NMR spectrum of $(C_6F_5)_2Te$ in $CDCl_3$.

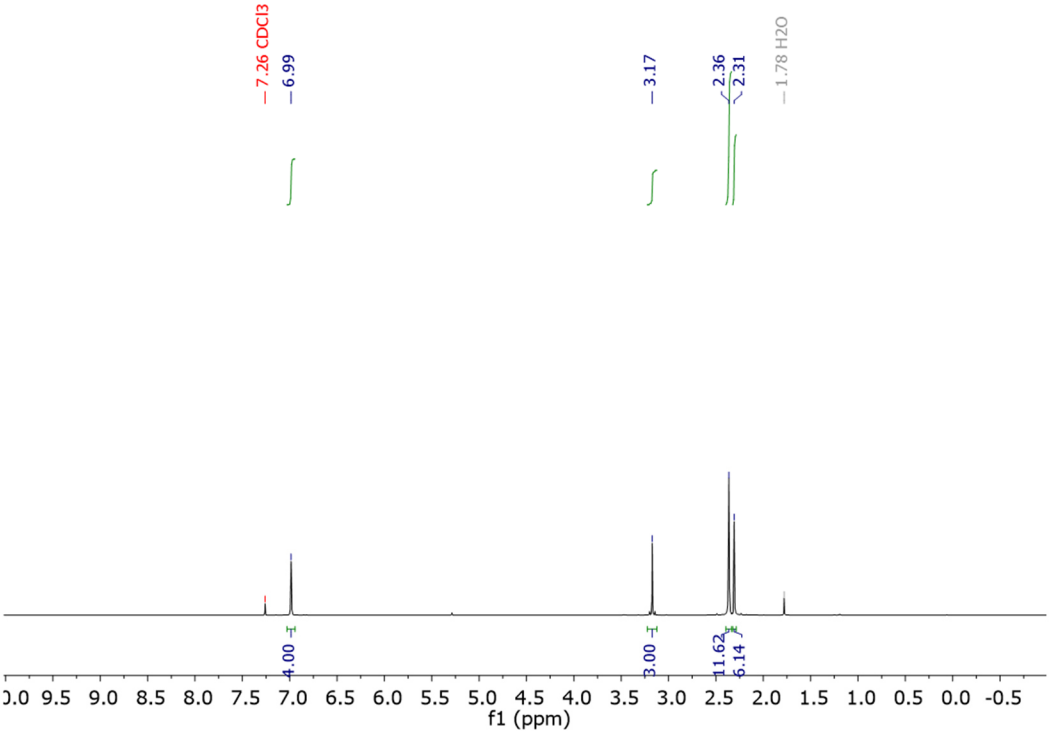

Figure S11. ^{1}H-NMR spectrum of [Mes_2TeMe][BF_4] ([**2**][BF_4]) in $CDCl_3$.

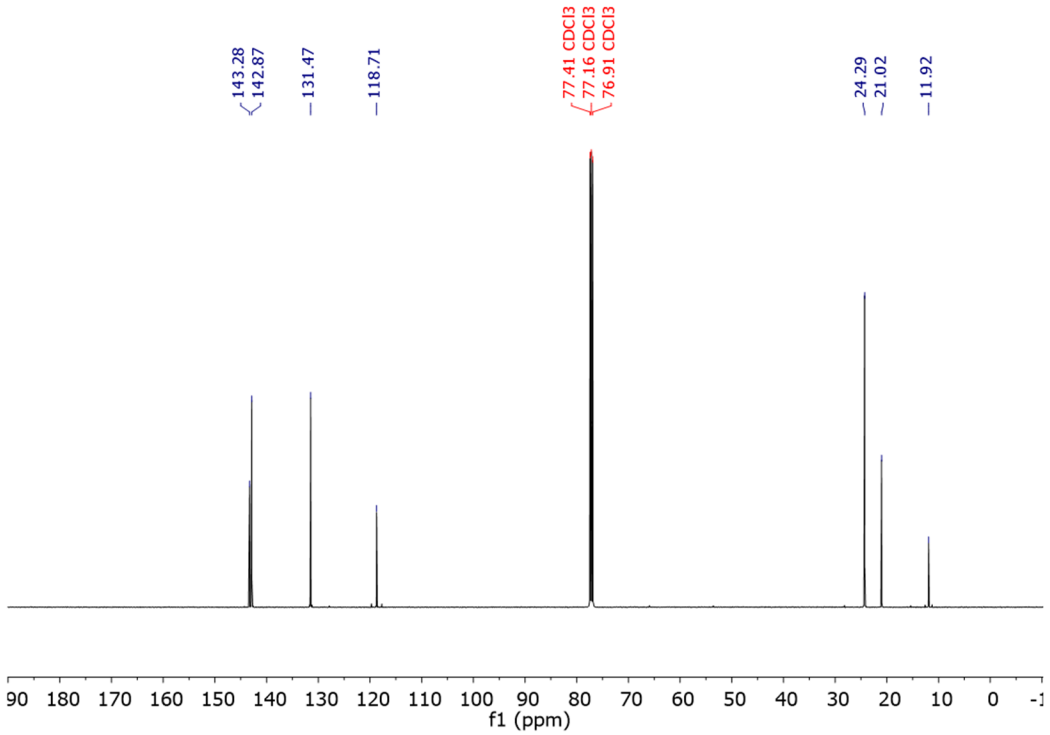

Figure S12. ^{13}C-NMR spectrum of [Mes_2TeMe][BF_4] ([**2**][BF_4]) in $CDCl_3$

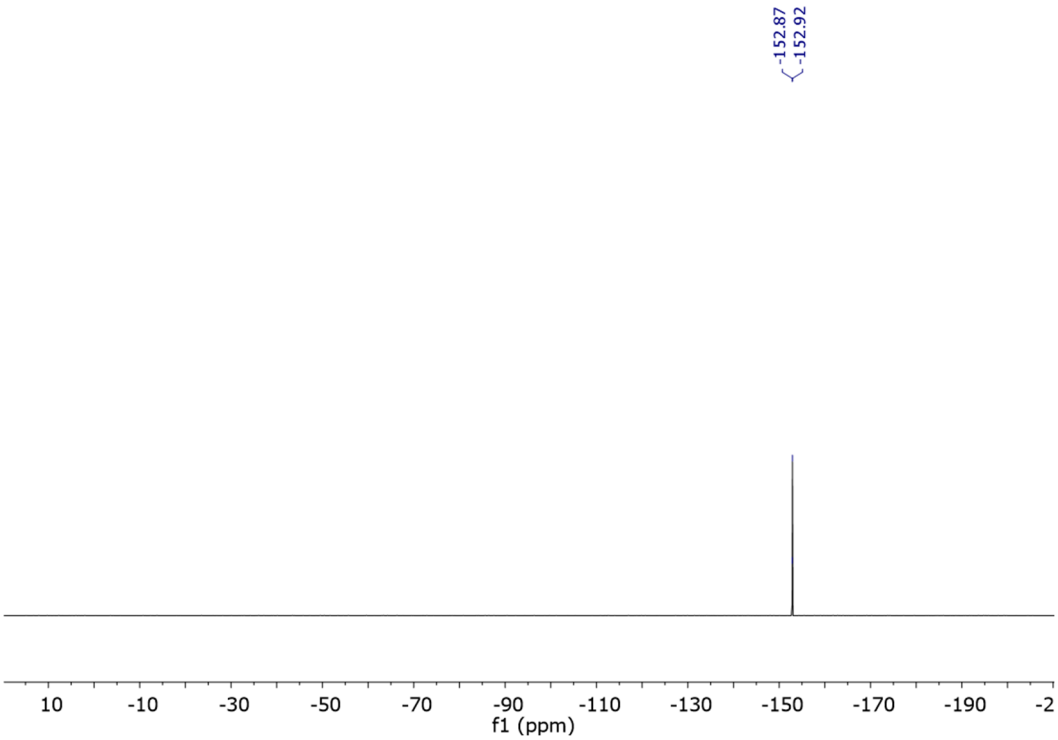

Figure S13. ^{19}F-NMR spectrum of [Mes_2TeMe][BF_4] ([**2**][BF_4]) in $CDCl_3$.

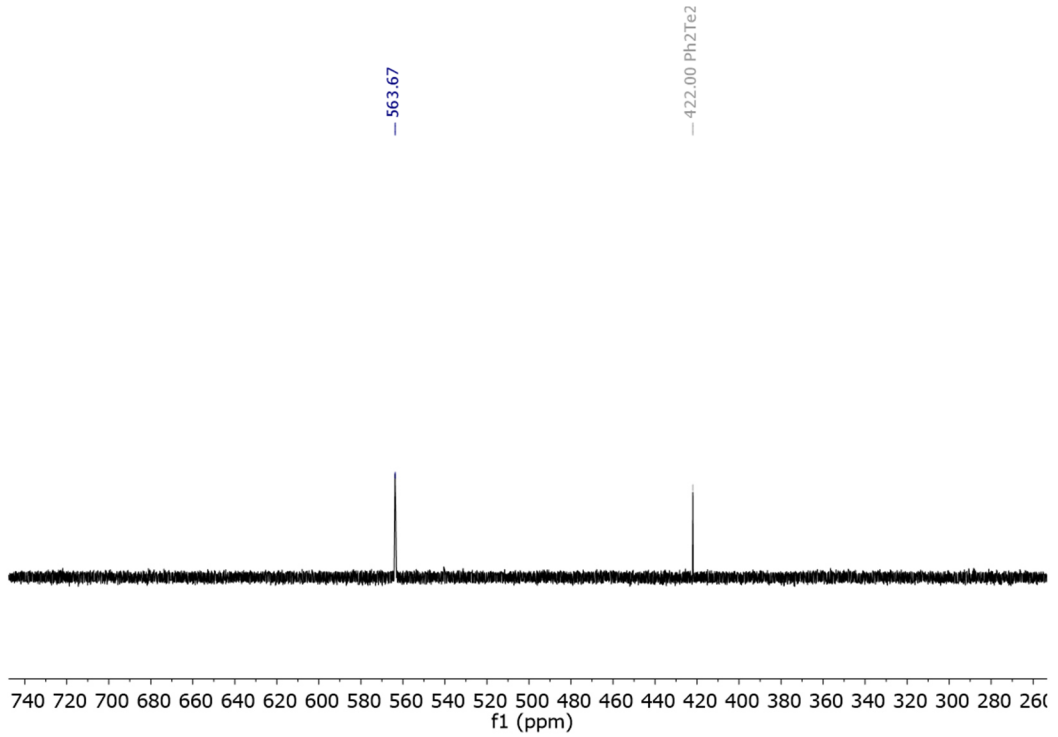

Figure S14. ^{125}Te-NMR spectrum of [Mes_2TeMe][BF_4] ([**2**][BF_4]) in $CDCl_3$.

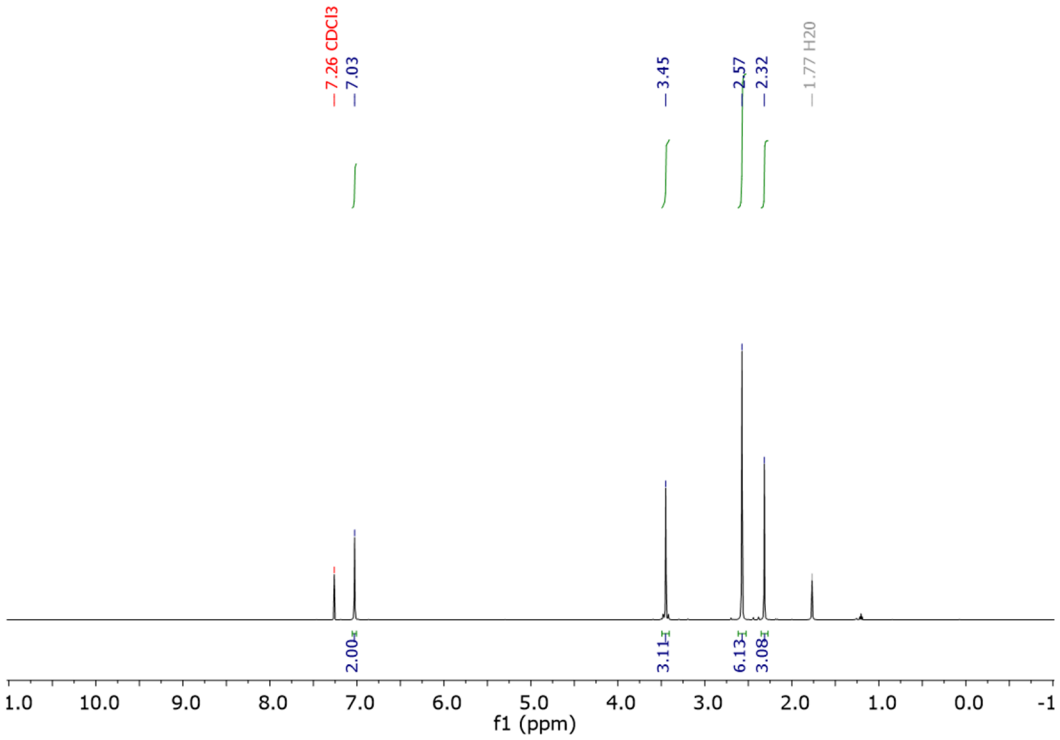

Figure S15. ^{1}H-NMR spectrum of [Mes(C_6F_5)TeMe][BF_4] ([**3**][BF_4]) in $CDCl_3$.

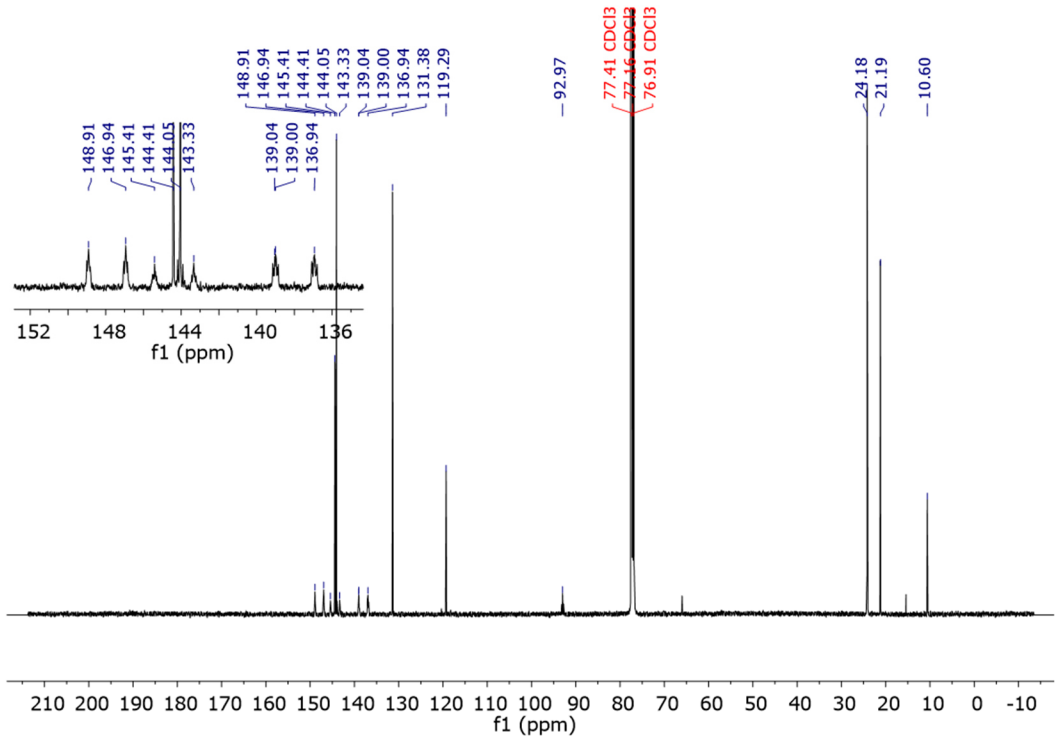

Figure S16. ^{13}C-NMR spectrum of [Mes(C_6F_5)TeMe][BF_4] ([**3**][BF_4]) in $CDCl_3$.

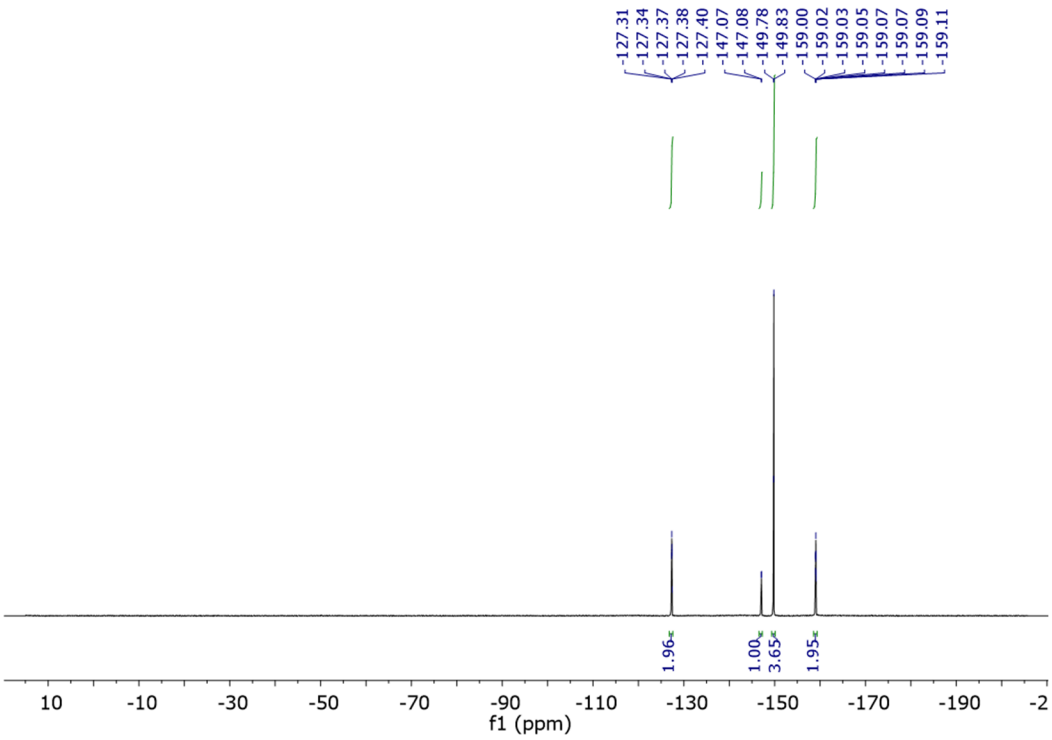

Figure S17. ^{19}F-NMR spectrum of [Mes(C_6F_5)TeMe][BF_4] ([**3**][BF_4]) in $CDCl_3$.

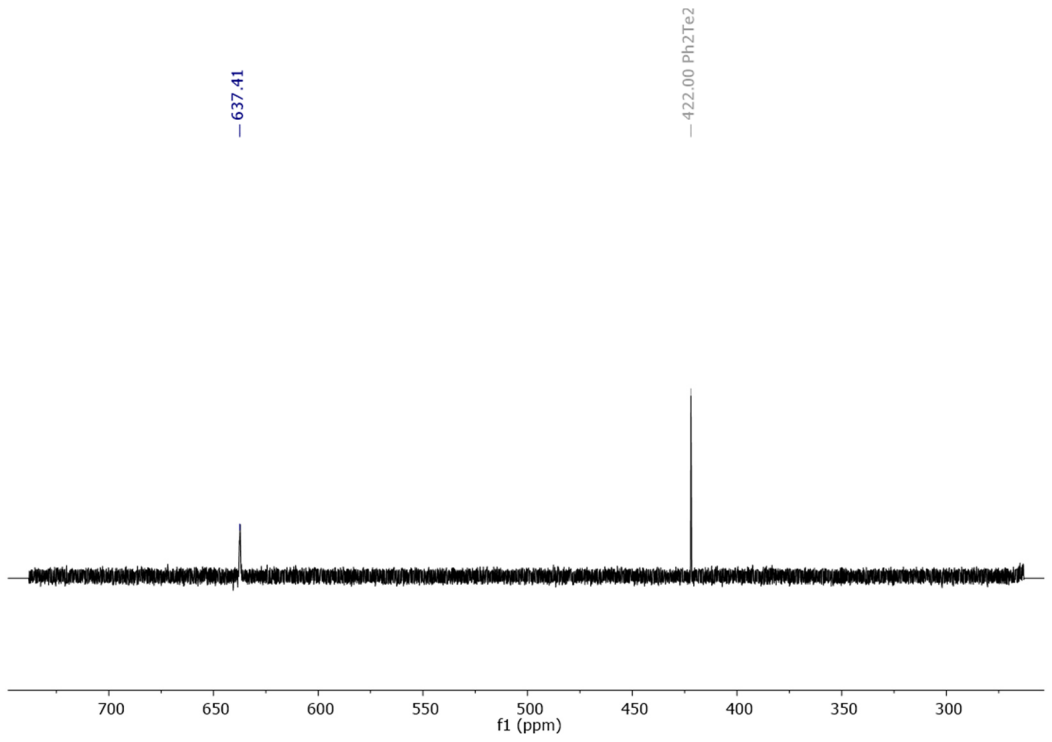

Figure S18. ^{125}Te-NMR spectrum of [Mes(C_6F_5)TeMe][BF_4] ([**3**][BF_4]) in $CDCl_3$.

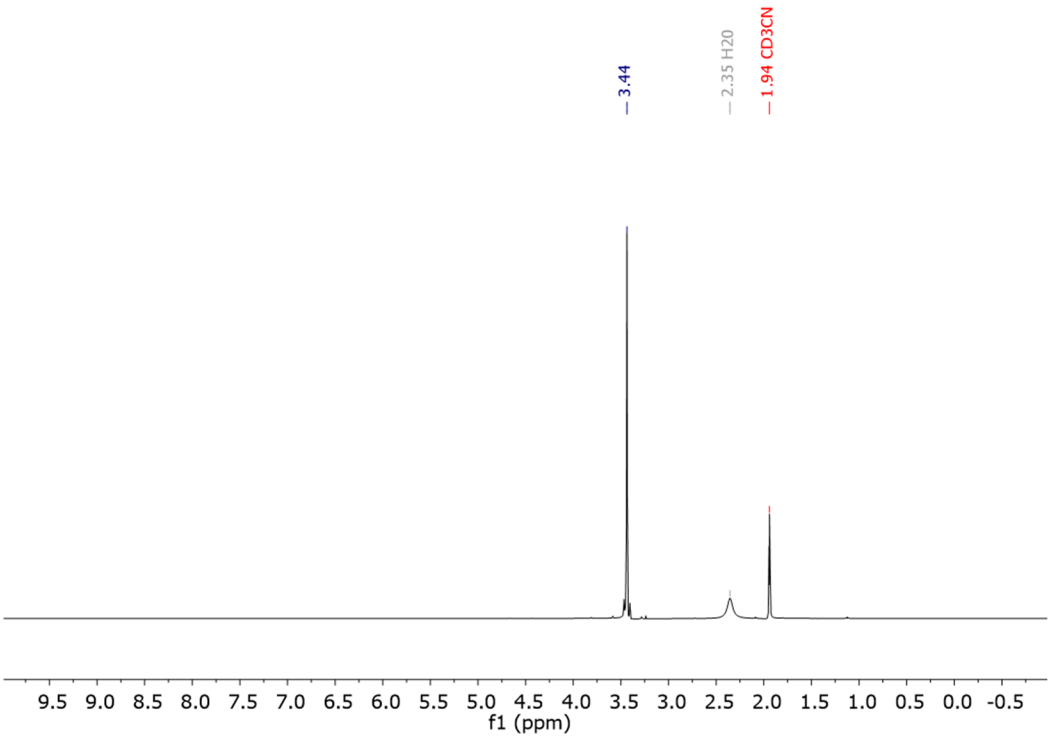

Figure S19. ^{1}H-NMR spectrum of $[(C_6F_5)_2TeMe][BF_4]$ ([**4**][BF_4]) in CD_3CN.

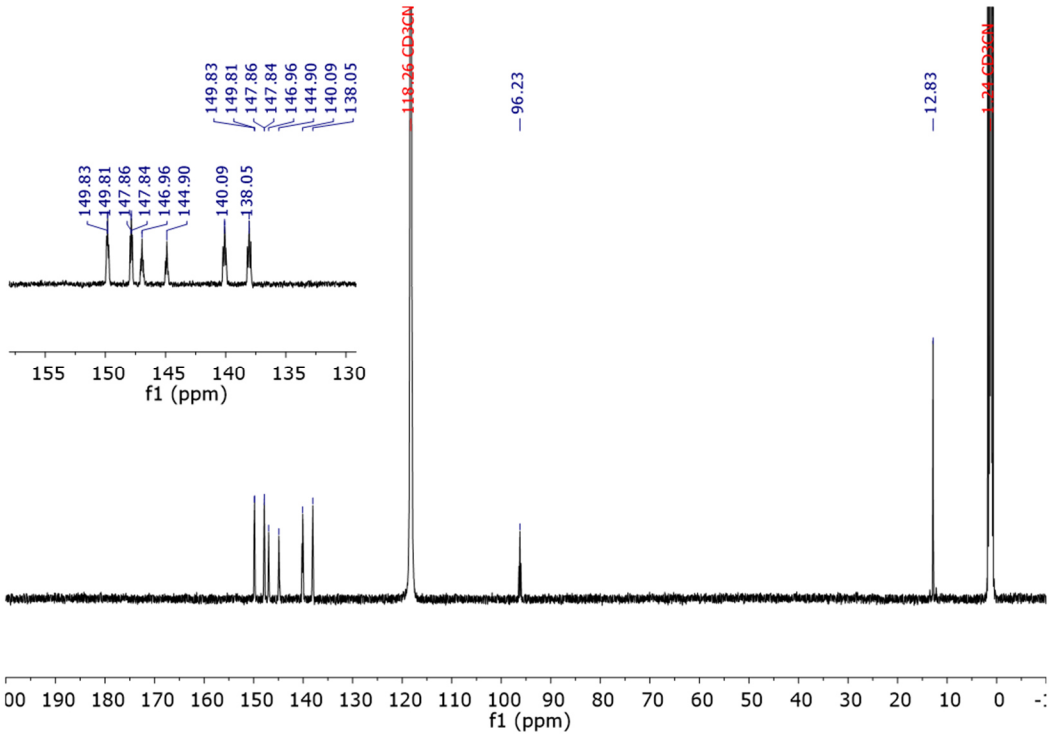

Figure S20. ^{13}C-NMR spectrum of $[(C_6F_5)_2TeMe][BF_4]$ ([**4**][BF_4]) in CD_3CN.

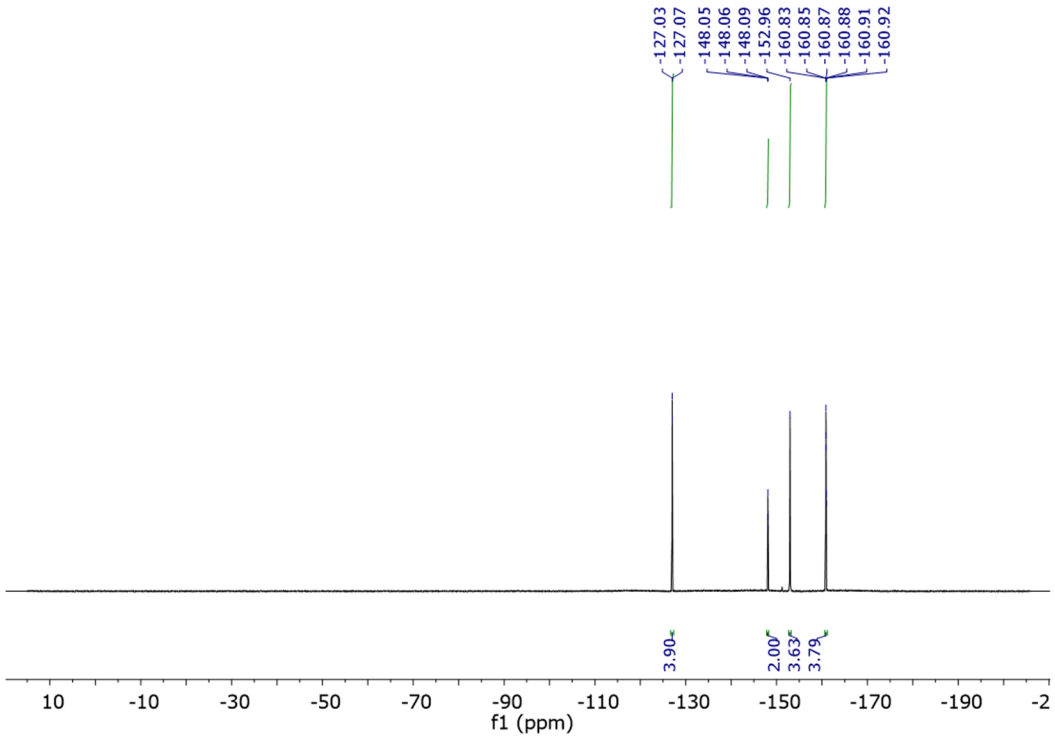

Figure S21. ^{19}F-NMR spectrum of $[(C_6F_5)_2TeMe][BF_4]$ ([**4**][BF_4]) in CD_3CN.

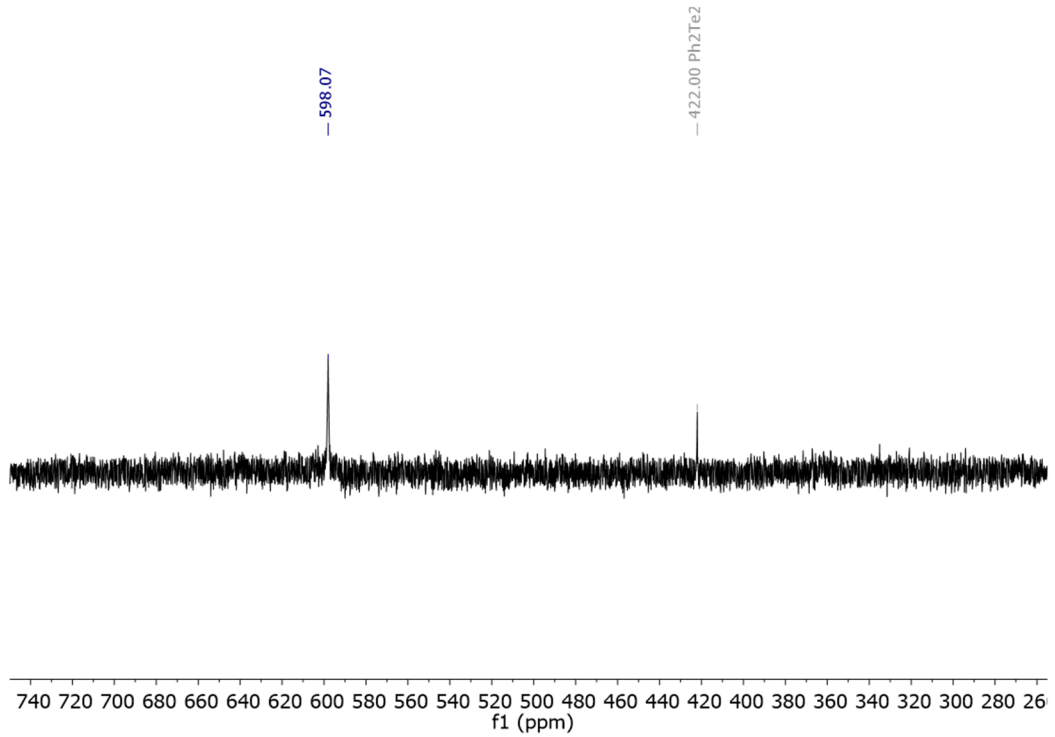

Figure S22. ^{125}Te-NMR spectrum of $[(C_6F_5)_2TeMe][BF_4]$ ([**4**][BF_4]) in CD_3CN.

2 Chloride ion binding studies

In a typical experiment, a TBACl (or Ph_4PCl) stock solution in CH_3CN (70 to 140 mM) was added by small increments (5-10 μL) to an NMR tube containing an MeCN solution (0.5 mL) of the tellurium derivative (3.5 to 3.9 mM). After mixing the solution by inverting the NMR tube upside down three times, the ^{19}F-NMR spectrum was recorded. The changes in chemical shift Δδ of the most responsive fluorine signal were used to plot binding isotherms which were fitted to the following equation:

$$\Delta\delta = (\Delta\delta_{max} /(c_0 \times V_0)) \times (0.5 \times (c_0 \times V_0 + c_{Cl} \times V_{Cl} + (V_0 + V_{Cl})/K_a) - 0.5 \times ((c_0 \times V_0 - c_{Cl} \times V_{Cl})^2 + 2 \times (c_0 \times V_0 + c_{Cl} \times V_{Cl}) \times (V_0 + V_{Cl})/K_a + ((V_0 + V_{Cl})/K_a)^2)^{0.5}) \quad \text{(S1)}$$

with:

c_0 = concentration of the host solution

V_0 = volume of host solution

c_{Cl} = volume of the TBACl (or Ph_4Cl) stock solution

V_{Cl} = volume of the TBACl (or Ph_4Cl) stock solution

K_a = binding constant

a)

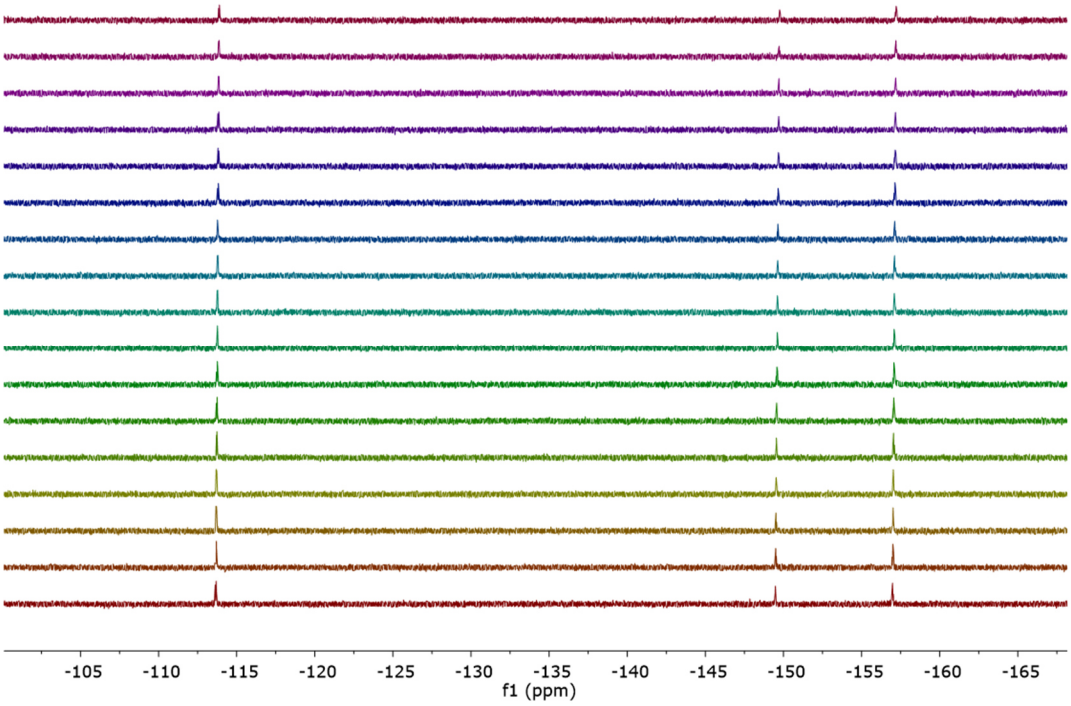

b)

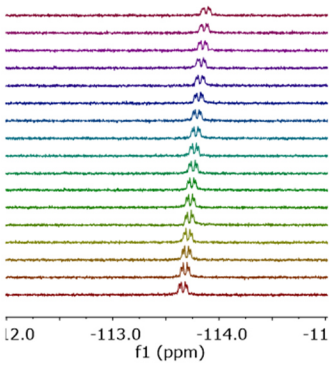

c)

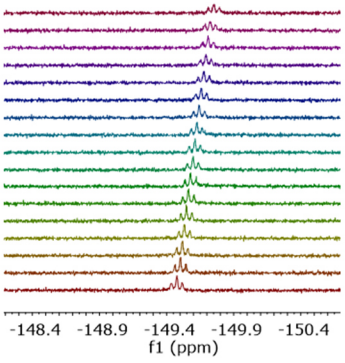

d)

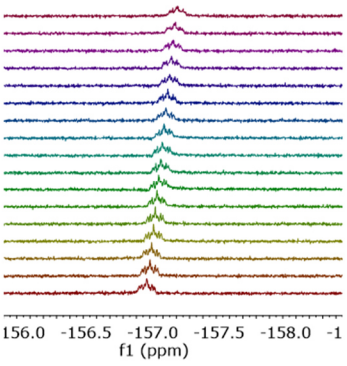

Figure S23. Changes observed in the ^{19}F-NMR spectrum of a 3.5 mM CH_3CN solution of C_6F_5TeMes upon incremental addition of TBACl. Panel a) shows the full spectra while panels b), c), and d) show close-ups of the *o*-F, *p*-F, *m*-F resonances, respectively. All three resonances showed only negligible changes in chemical shift ($\Delta\delta < 0.3$ ppm) upon addition until 8.9 equiv. of TBACl.

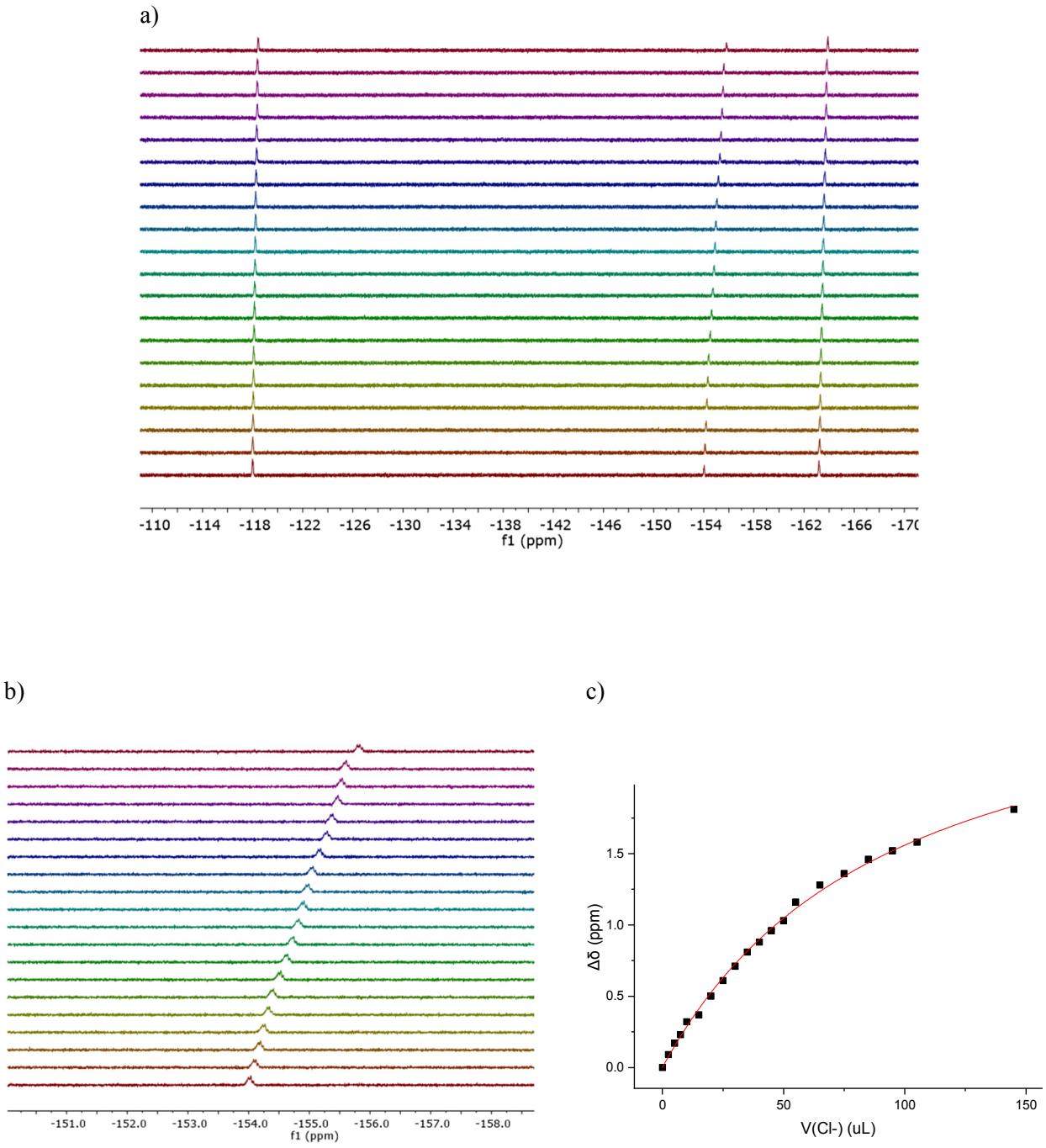

Figure S24. Changes observed in the ^{19}F-NMR spectrum of a 3.5 mM CH_3CN solution of $(C_6F_5)_2Te$ upon incremental addition of TBACl (140 mM in CH_3CN, bottom to up). Panel a) shows the full spectra while panel b) shows a close-up of the *p*-F resonance. Panel c) shows the fitting of the chemical shift change data according to a 1:1 binding isotherm (Equation S1). K_a = 35.4 ± 0.2 M^{-1}, $\Delta\delta_{max}$ = 3.56 ± 0.14 ppm, R^2 = 0.99798.

a)

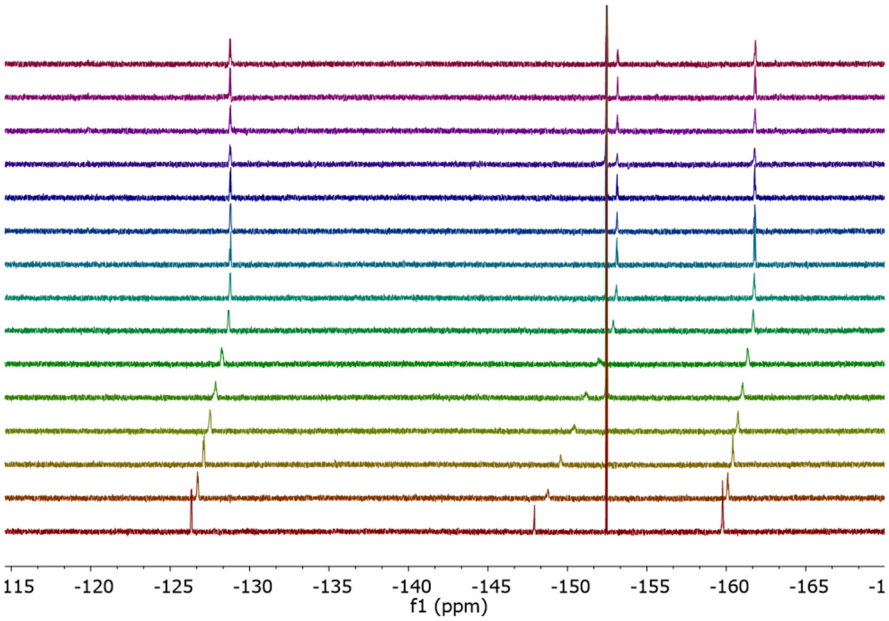

b)

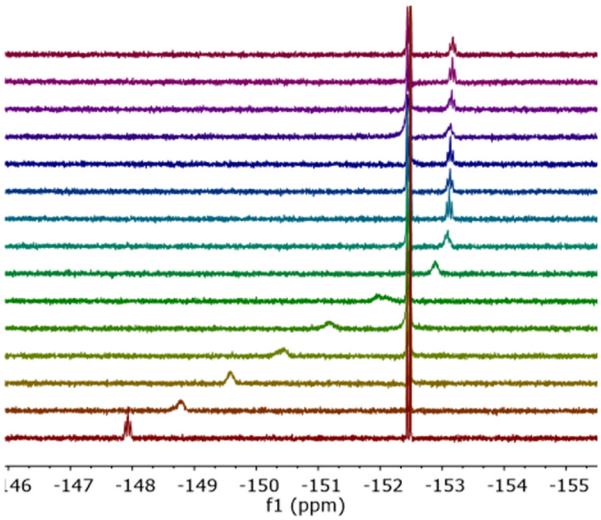

c)

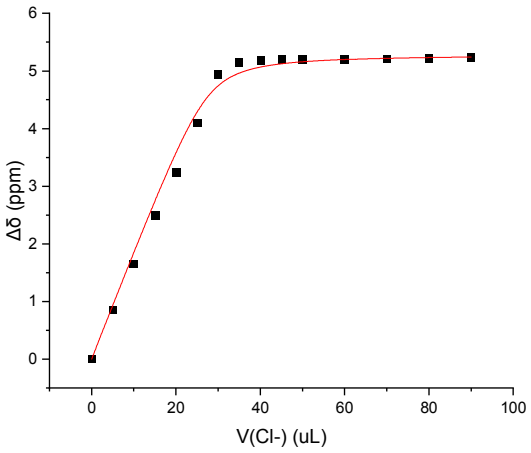

Figure S25. Changes observed in the ^{19}F-NMR spectrum of a 3.5 mM CH_3CN solution of $[C_6F_5TeMesMe][BF_4]$ ([**3**][BF_4]) upon incremental addition of TBACl (70 mM in CH_3CN, bottom to up). Panel a) shows the full spectra while panel b) shows a close-up of the *p*-F resonance. Panel c) shows the fitting of the chemical shift change data according to a 1:1 binding isotherm (Equation S1) with K_a = (1.26 ± 0.6) × 10^4 M^{-1}, $\Delta\delta_{max}$ = 5.23 ± 0.10, R^2 = 0.99205.

a)

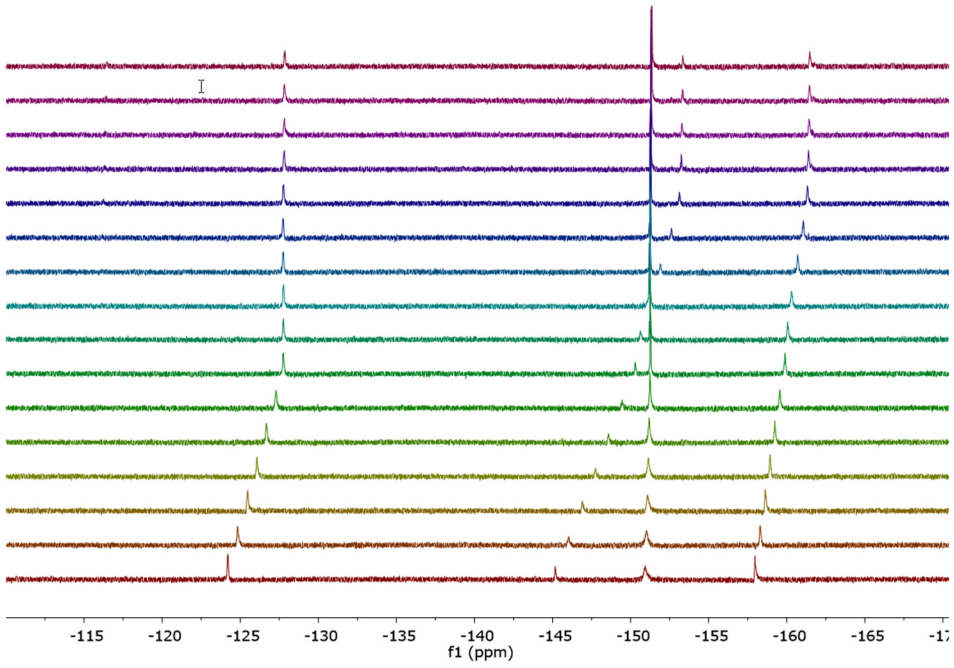

b)

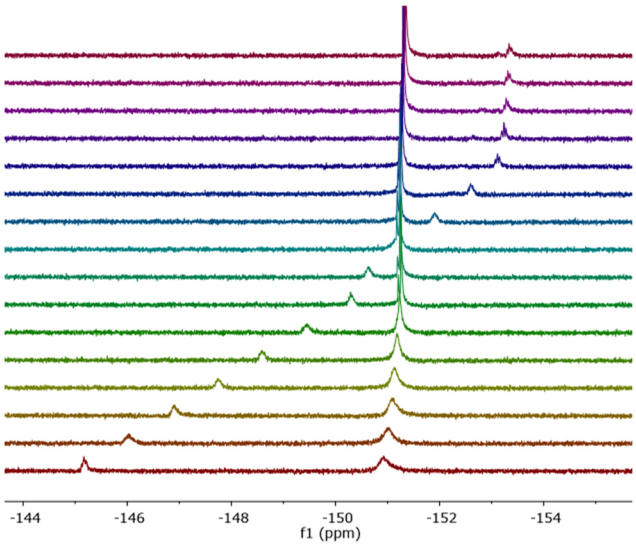

c)

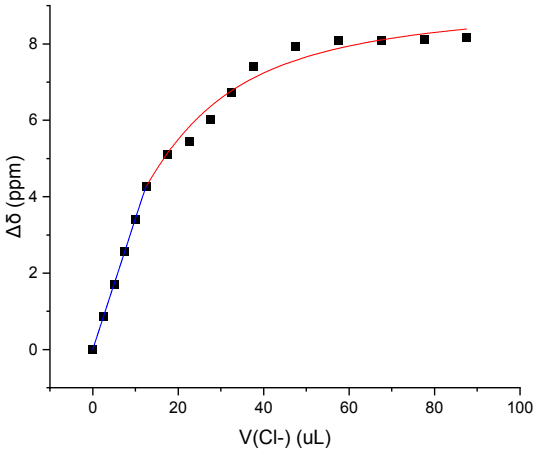

Figure S26. Changes observed in the ^{19}F-NMR spectrum of a 3.5 mM CH_3CN solution of $[(C_6F_5)_2TeMesMe][BF_4]$ ([**4**][BF_4]) upon incremental addition of TBACl (140 mM in CH_3CN, bottom to up). Panel a) shows the full spectra while panel b) shows a close-up of the *p*-F resonance. Panel c) shows the fitting of the chemical shift change data. The first six spectra which correspond to the addition of the first equivalent showed a linear variation of the chemical shift, indicating quantitative formation of the 1:1 adduct **4**-Cl ($K_1 > 10^5$ M^{-1}). The rest of the spectra were fitted to a 1:1 binding isotherm corresponding to **4**-Cl + Cl-↔ [**4**-Cl_2]$^-$ using equation S1. This fitting afforded $K_2 = (259 \pm 79) \times 10^5$ M^{-1}, $\Delta\delta_{max} = 5.15 \pm 0.50$, $R^2 = 0.96724$.

3 Anion transport studies

3.1 Vesicles preparation

EYPC-LUVs. The vesicles were prepared according to a previously established method.[7] A thin film of lipid was prepared by evaporating a solution of EYPC (45 mg) dissolved in $CHCl_3$ (2 mL). The film was dried under vacuum overnight. A buffered solution of KCl (1 mL, 300 mM KCl, 10 mM HEPES, pH = 7.2) was added to suspend the lipid film. The suspension was subjected to 9 freeze-thaw (liquid N_2 bath, 50 °C water bath) cycles and then extruded through a 200 nm polycarbonate membrane 33 times. After extrusion, the extravesicular component was removed through a size exclusion column (loaded with Sephadex G-50) using a buffer solution (300 mM KGluc, 10 mM HEPES, pH = 7.2) as the eluent.

DPPC-LUVs. The vesicles were prepared according to a previously established method.[8] A thin film of lipid was prepared by evaporating a solution of DPPC (32.5 mg) dissolved in a mixture of 1:1 MeOH/$CHCl_3$ (2 mL). The film was dried under vacuum overnight. A buffered solution of KCl (1 mL, 300 mM KCl, 10 mM HEPES, pH = 7.2) was added to suspend the lipid film at 50 °C. The suspension was subjected to 9 freeze-thaw cycles (liquid N_2 bath, 50 °C water bath) and then extruded 33 times through a 200 nm polycarbonate membrane at 50 °C. After extrusion, the extravesicular component was removed through a size exclusion column (loaded with Sephadex G-50) using a buffer solution (300 mM KGluc, 10 mM HEPES, pH = 7.2) as the eluent.

EYPC-LUVs loaded with 5(6)-carboxyfluorescein (CF). The vesicles were prepared according to a previously established method.[9] A thin film of lipid was prepared by evaporating a solution of EYPC (20 mg) dissolved in $CHCl_3$ (2 mL). The film was dried under vacuum overnight. A buffered solution (1 mL, 10 mM NaCl, 10 mM HEPES, 50 mM CF, pH = 7.4) was added to suspend the lipid film. The suspension was subjected to 9 freeze-thaw cycles (liquid N_2 bath, 50 °C water bath) and then extruded 33 times through a 200 nm polycarbonate membrane. After extrusion, the extravesicular component was removed through a size exclusion column (loaded with Sephadex G-50) using a buffer solution (100 mM NaCl, 10 mM HEPES, pH = 7.4) as the eluent.

3.2 Cl^- transport activity studies

The following assay was adapted from literature reports.[7] Vesicles containing KCl (300 mM buffered with 10 mM HEPES, pH = 7.2) were suspended in an external buffer (300 mM KGluc., 10 mM HEPES, pH = 7.2) affording a 5 mL solution with a lipid concentration of 0.7 mM. A valinomycin solution (1 mM in DMSO, 3.5 μL, 0.1 mol% with respect to lipid concentration) was injected at t = 0 s. The transporter

solution (10 mM in DMSO, 7 µL, 2 mol% with respect to lipid concentration) was added at t = 30 s. The chloride concentration was monitored using a chloride selective electrode, which had been calibrated by standard chloride solution. At t = 300 s, 50 µL of a Triton X solution (10:1:0.1 H_2O:DMSO:Triton X (v/v/v)) was added to lyse to vesicles, leading to full release of the chloride cargo. A final reading was recorded at t= 420 s and assigned a value of 100% chloride efflux.

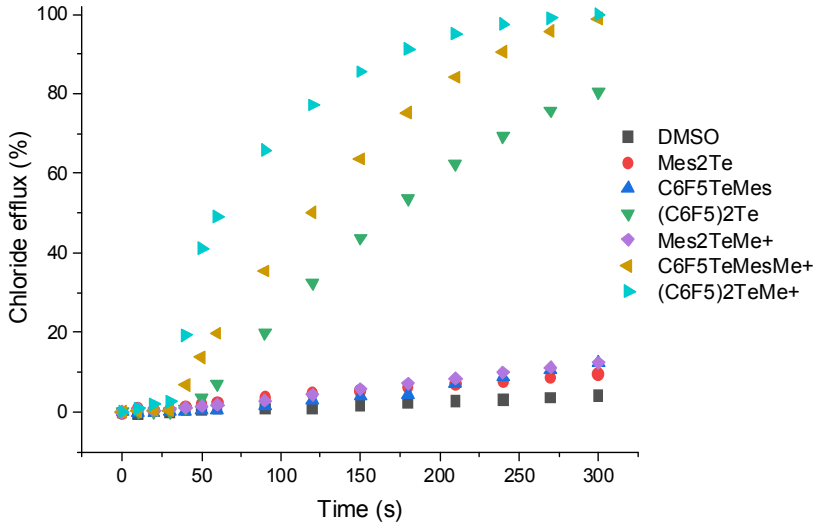

Figure S27. Chloride efflux from EYPC vesicles triggered by the addition of a DMSO solution of the transporter (7 µL, 2 mol% with respect to lipid concentration) in the presence of valinomycin (0.2 mol%). The chloride efflux was monitored using a chloride selective electrode.

3.3 Hill analyses of the most active transporters

Hill analyses were performed on the most active transporters (**1**, **4**, **5**) using the assay described above but with different concentrations of the transporters. The chloride efflux percentage at 270 s was recorded (Y) and plotted versus the transporter concentration (c) according to the following Hill equation:

$$Y = Y_0 + (Y_m - Y_0)\frac{c^n}{c^n + EC_{50}{}^n} \qquad \text{(S2)}$$

where Y_m = maximum chloride efflux (100%); Y_0 = chloride efflux at 270 s without transporter; EC_{50} = effective concentration of the transporter; n = Hill coefficient.

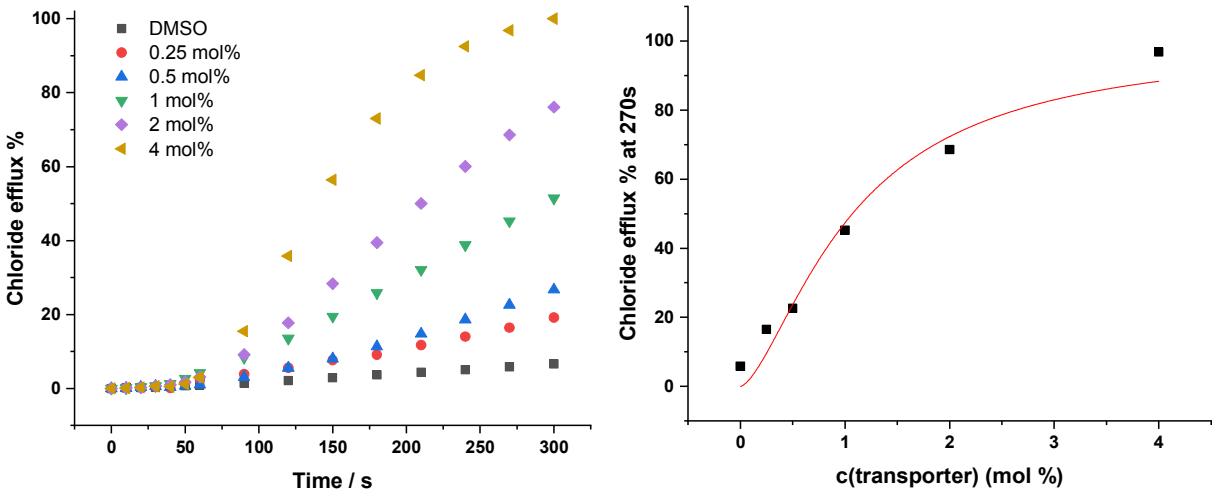

Figure S28. Left: chloride efflux from EYPC vesicles triggered by the addition of a DMSO solution of $(C_6F_5)_2Te$ (7 µL, 0.25 mol%, 0.5 mol%, 1 mol%, 2 mol % and 4 mol% with respect to lipid concentration) in the presence of valinomycin (0.2 mol%). Right: Hill analysis: fitting of the chloride efflux at 270s versus the concentration of the transporter using equation S2. The fitting afforded EC_{50} = 1.07 ± 0.12 mol%, n = 1.54 ± 0.25, R^2 = 0.97151.

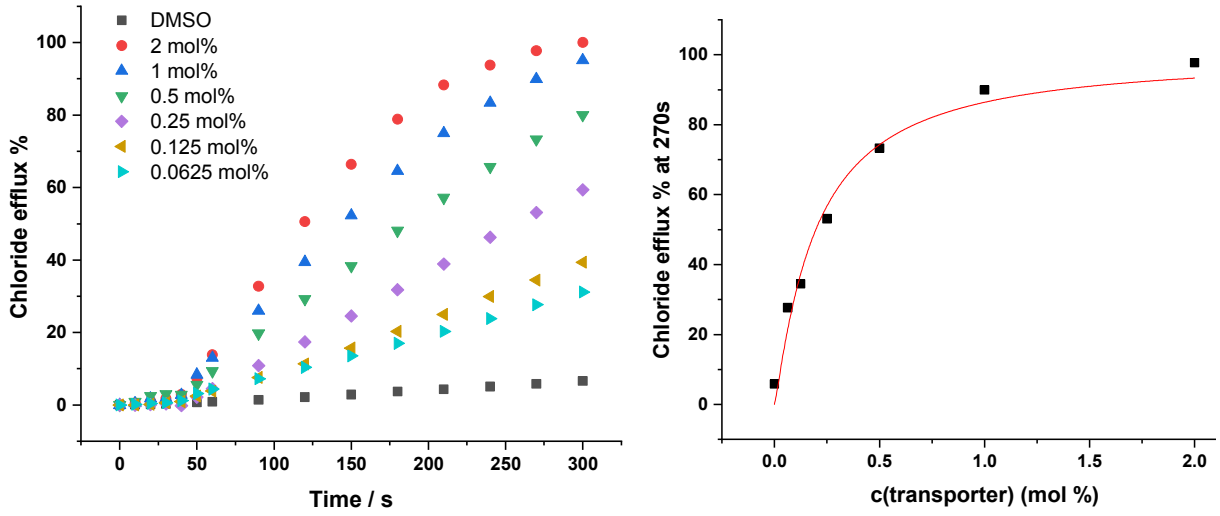

Figure S29. Left: chloride efflux from EYPC vesicles triggered by the addition of a DMSO solution of [**3**][BF_4] (7 µL, 0.0625 mol%, 0.125 mol%, 0.25 mol%, 0.5 mol %, 1 mol% and 2 mol% with respect to lipid concentration) in the presence of valinomycin (0.2 mol%). Right: Hill analysis: fitting of the chloride efflux at 270s versus the concentration of the transporter using equation S2. The fitting afforded: EC_{50} = 0.20 ± 0.02 mol%, n = 1.14 ± 0.14, R^2 = 0.9815.

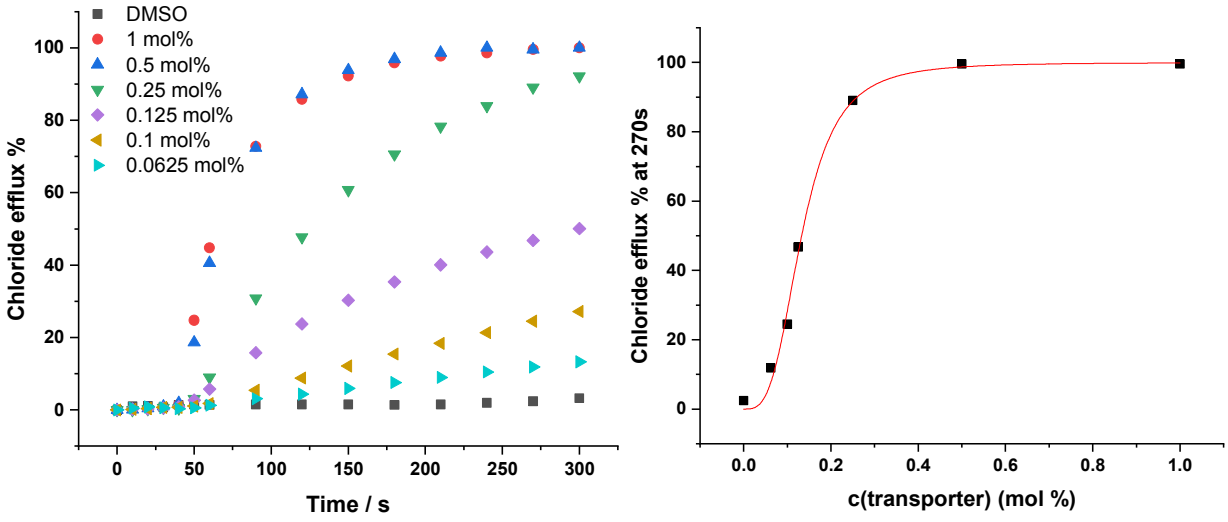

Figure S30. Left: chloride efflux from EYPC vesicles triggered by the addition of a DMSO solution of [**4**][BF_4] (7 µL, 0.0625 mol%, 0.125 mol%, 0.25 mol%, 0.5 mol %, and 1 mol% with respect to lipid concentration) in the presence of valinomycin (0.2 mol%). Right: Hill analysis: fitting of the chloride efflux at 270s versus the concentration of the transporter using equation S2. The fitting afforded: EC_{50} = 0.133 ± 0.004 mol%, n = 3.28 ± 0.30, R^2 = 0.99622.

3.4 Temperature-dependent Cl^- transport using DPPC-LUVs

Vesicles containing KCl (300 mM buffered with 10 mM HEPES, pH = 7.2) were suspended in an external buffer (300 mM KGluc., 10 mM HEPES, pH = 7.2) to afford a 5 mL solution with a lipid concentration of 0.7 mM. The solution was kept at 25 °C or warmed 45 °C. The rest of the transport experiment followed the protocol used with the EYPC vesicles.

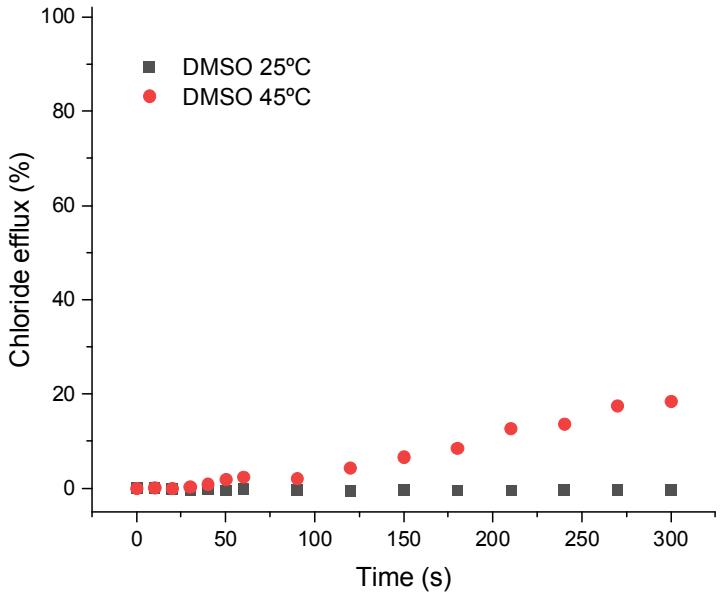

Figure S31. Chloride efflux from DPPC vesicles triggered by the addition of DMSO (7 µL) in the presence of valinomycin (0.2 mol%) at 25 °C (grey) and 45 °C (red).

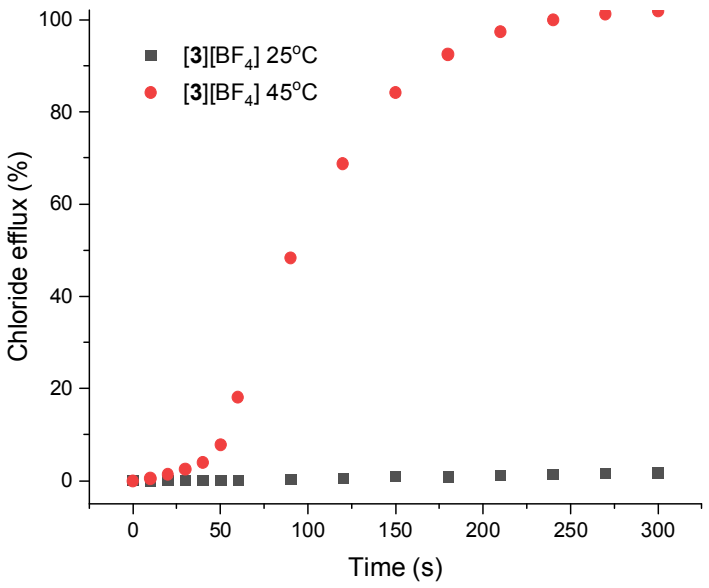

Figure S32. Chloride efflux from DPPC vesicles triggered by the addition of a DMSO solution of [**3**][BF_4] (7 µL) in the presence of valinomycin (0.2 mol%) at 25 °C (grey) and 45 °C (red).

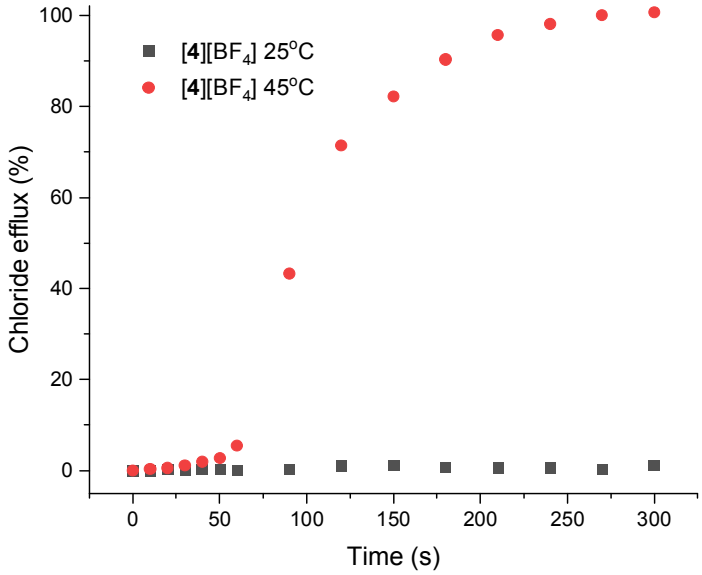

Figure S33. Chloride efflux from DPPC vesicles triggered by the addition of a DMSO solution of [**4**][BF_4] (7 µL) in the presence of valinomycin (0.2 mol%) at 25 °C (grey) and 45 °C (red).

3.5 Cl^- transport initial rate analysis

The initial rate (k_{ini}) of chloride efflux was obtained by non-linear fitting of the mearsured chloride efflux (%) versus time (s) after the addition of the transporter solution (30s to 300 s) with the following asymptotic model function using the Origin software:

$$y = a - b \bullet c^{(x)}$$

y is chloride efflux percentage (%)

x = t -30 (x is set to 0 at the time at which the transporter is added) (s)

k_{ini} is defined as the slope at x = 0. It can be derived as $k_{ini} = -b \bullet \ln(c)$ ($\%\bullet s^{-1}$).

For $(C_6F_5)_2Te$, which has a lower activity, the initial rate was determined by a linear fitting of the chloride efflux (%) versus time (s) of the early stage of the efflux using the linear function below:

$$y = a + b \bullet x$$

y is chloride efflux percentage (%)

x is time (s)

k_{ini} is equal to b ($\%\bullet s^{-1}$)

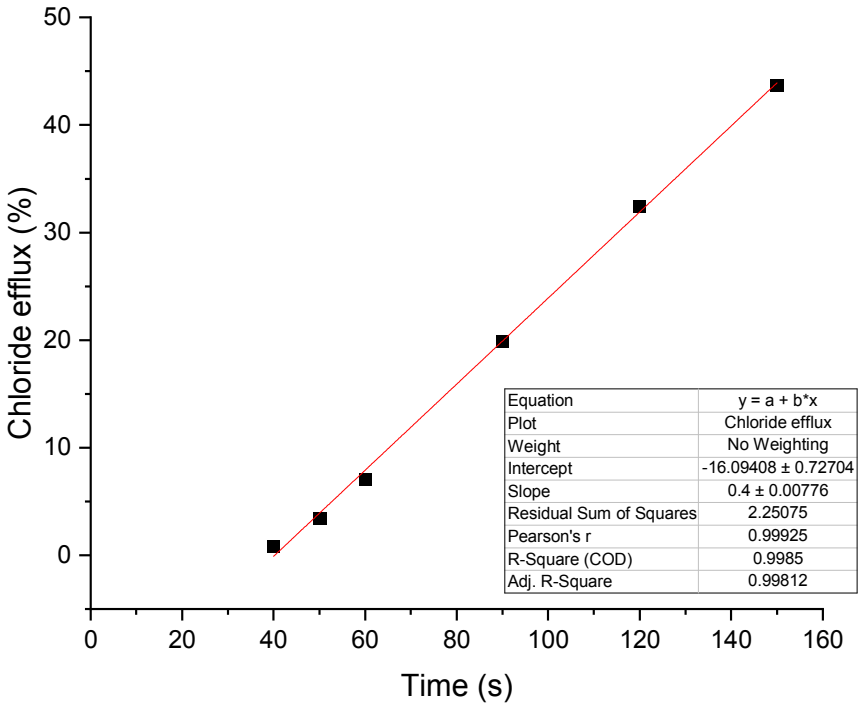

Figure S34. Fitting used to calculate k_{ini} when $(C_6F_5)_2Te$ is used as a transporter (2.0 mol% with respect to the lipid concentration), in the presence of valinomycin, using EYPC vesilces. The EYPC vesicles were loaded with KCl (300 mM) and suspended in KGlc (300 mM) buffered to pH 7.2. The fitting affords: k_{ini} = b = 0.40 %•s^{-1}.

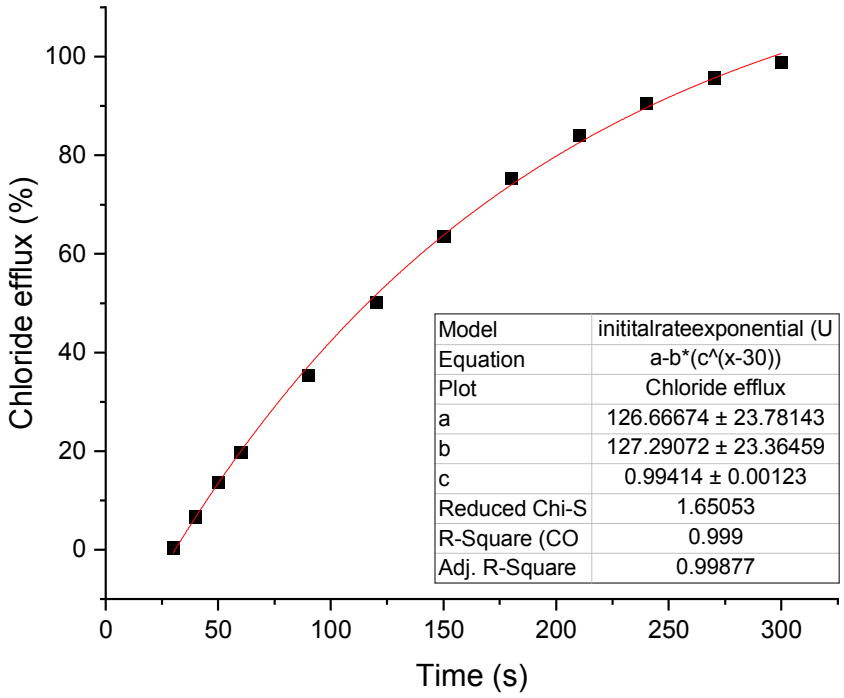

Figure S35. Fitting used to calculate k_{ini} when $[\mathbf{3}]^+$ is used as a transporter (2.0 mol% with respect to the lipid concentration), in the presence of valinomycin, using EYPC vesilces. The EYPC vesicles were loaded with KCl (300 mM) and suspended in KGlc (300 mM) buffered to pH 7.2. The fitting affords: k_{ini} = -b•ln(c) = 0.748 %•s^{-1}.

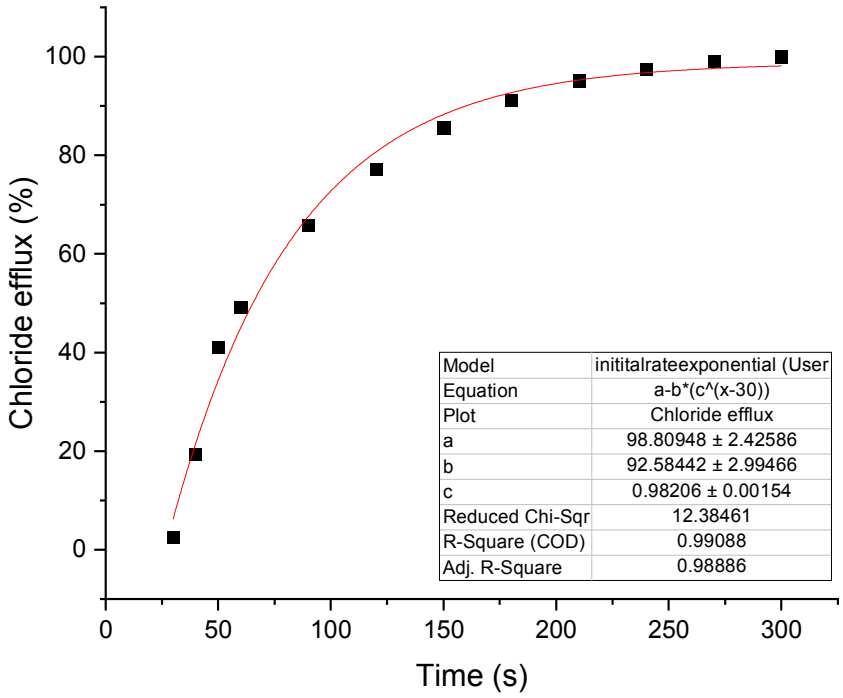

Figure S36. Fitting used to calculate k_{ini} when $[\mathbf{4}]^+$ is used as a transporter (2.0 mol% with respect to the lipid concentration), in the presence of valinomycin, using EYPC vesilces. The EYPC vesicles were loaded with KCl (300 mM) and suspended in KGlc (300 mM) buffered to pH 7.2. The fitting affords: k_{ini} = -b•ln(c) = 1.68 %•s^{-1}.

3.6 Leakage tests using EYPC-LUVs loaded with 5(6)-carboxyfluorescein (CF)

Vesicles loaded with a buffered CF solution (10 mM NaCl, 50 mM CF, 10 mM HEPES, pH = 7.4) were added to a fluorescence cuvette containing a buffered saline solution (100 mM NaCl, 10 mM HEPES, pH = 7.4) to afford a solution (3 mL) with a final lipid concentration of 0.1 mM. The cuvette was transferred into the fluorescence spectrometer. The solution was irradiated at λ_{ex} =492 nm and the emission intensity was monitored at λ_{em} = 517 nm. The transporter was added at t = 50 s as a DMSO solution. The vesicles were lysed at t= 350 s by addition of a triton X-100 solution (50 µL, 10:1:0.1 H_2O:DMSO:Triton X (v/v/v)). A final intensity reading was recorded at t = 420 s. The fluorescence intensities I_t was normalized to fractional intensities I_{rel} using the following equation:

$$I_{rel} = (I_t - I_0)/(I_\infty - I_0)$$

Where $I_0 = I_t$ at t = 50 s and $I_\infty = I_t$ at t = 420 s.

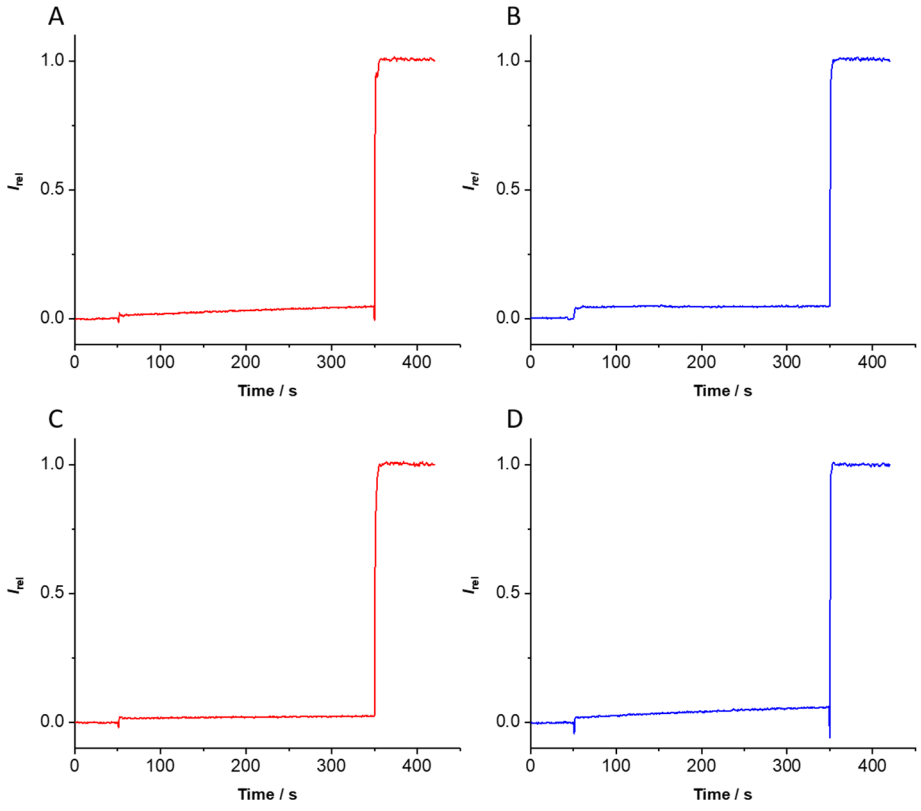

Figure S37. Change in fluorescence intensities I_{rel} (λ_{ex} =492 nm, λ_{em} = 517 nm) with addition of transporter solution (A: [**3**]BF_4, 0.4 mol%; B: [**3**]BF_4, 1 mol%; C: [**4**]BF_4, 0.4 mol%; D: [**4**]BF_4, 1 mol%). All concentrations are with respect to lipid concentration) at 50 s and triton X-100 solution at 350 s using vesicles loaded with 5(6)-carboxyfluorescein (CF).

4 Stability tests of the telluronium cations in D_2O/d_6-DMSO mixture

The telluronium salts were dissolved in a solution consisting of D_2O and d_6-DMSO (5:1 vol.). The final telluronium salt concentration was ~18.2 mM. These solution were analyzed by NMR over the course of 1 hour. Representative spectra are provided in Figure S38-40.

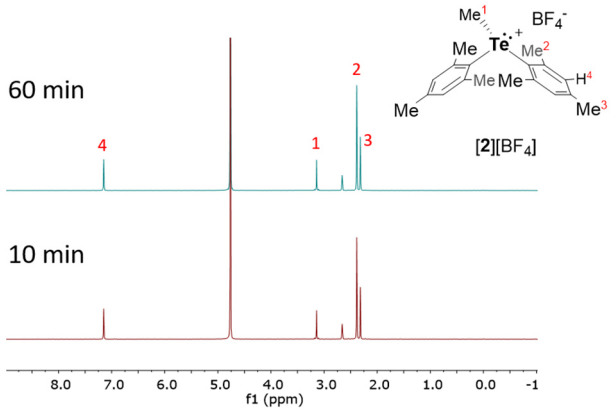

Figure S38. $^1/d_6$-DMSO, 10 min and 60 min after mixing.

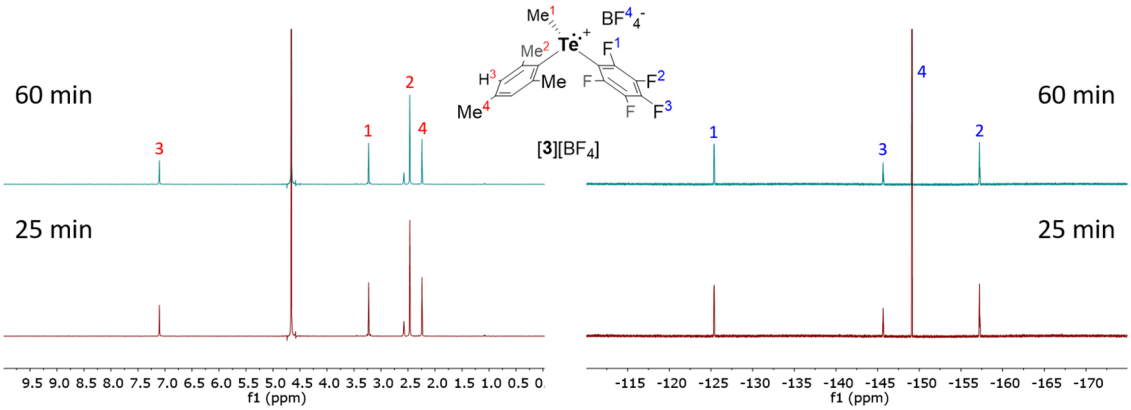

Figure S39. $^1/d_6$-DMSO, 25 min and 60 min after the mixing.

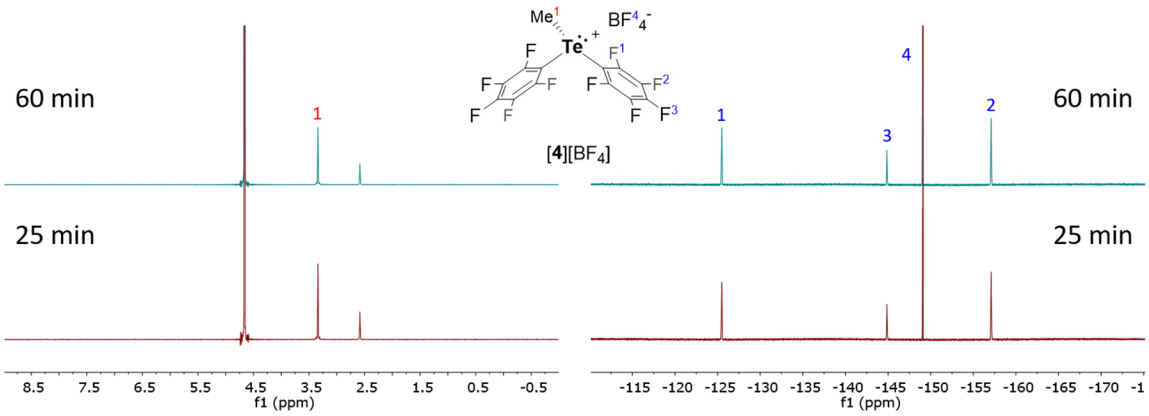

Figure S40. $^{1}/d_{6}$-DMSO, 25 min and 60 min after mixing.

5 X-ray crystallographic data

All crystallographic measurements were performed at 110(2) K using a Brucker D8 QUEST diffractometer (graphite monochromated Mo-Kα radiation, λ = 0.71073 Å). In each case, a specimen of suitable size and quality was selected and mounted onto a nylon loop. The semiempirical method SADABS was applied for absorption correction.[10] The structures were solved by direct methods and refined by the full-matrix least-squares technique against F^2 with the anisotropic temperature parameters for all non-hydrogen atoms. All H-atoms were geometrically placed and refined in riding model approximation. Data reduction and further calculations were performed using the Bruker SAINTplus and SHELXTL program packages.[11] Structure refinement was performed on Olex2.[12] The results of these X-ray measurments are provided as CIF files. CCDC 2004978-2004980 contain the supplementary crystallographic data for this paper.

6 Computational data

6.1 Methods

All computations were carried out using density functional theory (DFT) methods embedded in the Gaussian 16 program.[13] Optimization and frequency calculations were performed with the M062X[14] functional and mixed basis sets (cc-pVTZ-PP[15] with pseudopotential ECP28MDF[15] for Te; 6-31g(d') for C, H; 6-31+g(d') for F) starting from the crystal structure geometry (the counter anion BF_4^- was omitted for the calculation of telluronium cation). Cartesian coordinates of the optimized structure are provided below. No imaginary frequencies were found for the all of the optimized structures except for compound Mes(C_6F_5)Te (only one small negative frequency was found representing the rotation of the para-methyl group on the mesityl substituent), confirming that a local minimum on the potential energy hypersurface had been reached. Solvation calculations were performed on the optimized structure in gas phase using SMD model and water as the solvent. Same functional and basis sets were used as in gas phase calculations Optimized structures and electrostatic potential (ESP) maps were visualized by Gaussian View. Local maxima of electrostatic potential ($V_{s,max}$) are determined with multiwfn software [16] and are reported in kcal•mol^{-1}.

6.2 Optimized structures and coordinates of the tellurium compounds

Table S1. Cartesian coordinates of the optimized structure of Mes_2Te using M062X functional.

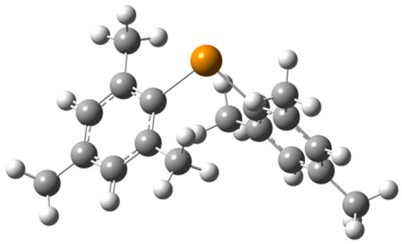

Te	-0.000000	-1.714400	-0.000100	C	-1.575500	-0.296700	-0.214700
C	1.575500	-0.296800	0.214500	C	-2.697600	-0.388200	0.633500
C	2.697600	-0.388100	-0.633600	C	-3.707800	0.565900	0.517600
C	3.707700	0.566000	-0.517700	H	-4.574500	0.497000	1.174700
H	4.574300	0.497300	-1.174900	C	-3.636600	1.608500	-0.407300
C	3.636600	1.608400	0.407400	C	-2.525200	1.667200	-1.240900
C	2.525200	1.666900	1.241200	H	-2.455500	2.466300	-1.978100
H	2.455600	2.465900	1.978500	C	-1.489100	0.727800	-1.173200
C	1.489200	0.727600	1.173400	C	-2.840600	-1.473600	1.672700
C	2.840600	-1.473400	-1.672900	H	-3.794400	-1.376700	2.200100
H	3.794500	-1.376500	-2.200200	H	-2.030200	-1.425400	2.410100
H	2.030300	-1.425000	-2.410500	H	-2.803500	-2.474000	1.225600
H	2.803300	-2.473800	-1.225900	C	-4.745300	2.625800	-0.499800
C	4.745200	2.625800	0.500000	H	-5.683500	2.158000	-0.821500
H	5.683500	2.157900	0.821500	H	-4.501400	3.417300	-1.215100
H	4.501400	3.417100	1.215500	H	-4.932800	3.093700	0.473600
H	4.932600	3.093900	-0.473300	C	-0.332400	0.876100	-2.129700
C	0.332600	0.875400	2.130100	H	-0.607700	1.535400	-2.958700
H	0.607400	1.535700	2.958500	H	-0.032300	-0.093900	-2.542900
H	0.033700	-0.094700	2.544100	H	0.548700	1.302700	-1.634600
H	-0.549100	1.300600	1.635000				

Table S2. Cartesian coordinates of the optimized structure of Mes(C_6F_5)Te (**1**) using M062X functional.

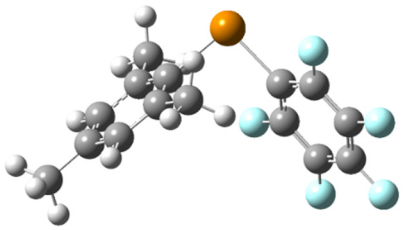

Te	0.409100	-1.818900	-0.399400	H	3.019800	-1.565200	-2.233500
F	-0.289400	0.949900	-1.902800	H	3.659700	-0.010300	-2.785300
F	-2.328100	2.684400	-1.703100	H	1.906400	-0.295500	-2.744900
F	-4.364300	2.202200	0.021900	C	1.851000	-0.349500	0.135600
F	-4.346600	-0.031200	1.561800	C	-1.227400	-0.476300	-0.265200
F	-2.310200	-1.771100	1.393300	C	3.744500	1.022600	-0.434900
C	2.803600	1.150700	1.760000	H	4.487400	1.345300	-1.163200
H	2.803900	1.571000	2.764700	C	0.847400	-0.218500	2.493100
C	3.757300	1.582400	0.842300	H	-0.158100	0.152100	2.255800
C	4.764500	2.642400	1.206900	H	1.131600	0.195100	3.465200
H	4.446600	3.623700	0.833500	H	0.772700	-1.307200	2.585600
H	5.744500	2.427100	0.768100	C	-3.349700	0.196900	0.713500
H	4.883900	2.722900	2.291900	C	-1.267800	0.679500	-1.040000
C	2.804700	0.063400	-0.814000	C	-2.287800	-0.693300	0.608600
C	1.844900	0.186500	1.436300	C	-3.359300	1.342700	-0.071000
C	2.850300	-0.482300	-2.220700	C	-2.313700	1.588500	-0.951700

Note: only one small imaginary frequency (40 Hz) was found as the rotation of the para-methyl group on the mesityl substituent group with respect to the mesityl plane.

Table S3. Cartesian coordinates of the optimized structure of $(C_6F_5)_2Te$ using M062X functional

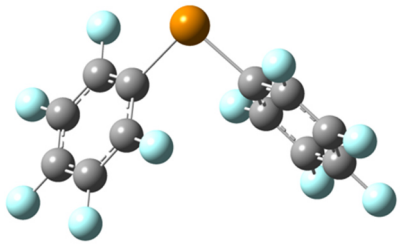

Te	-0.000000	-2.035500	-0.000000	C	-2.348700	1.440500	-1.289800
C	1.506500	-0.569800	0.217400	F	-2.800900	-1.506800	1.522500
C	-1.506500	-0.569800	-0.217400	C	-3.611500	0.416700	0.485700
C	1.389500	0.444900	1.163200	F	2.212900	2.400700	2.195100
C	2.632100	-0.562400	-0.599800	C	3.464900	1.421800	0.462200
C	-1.389400	0.445000	-1.163100	F	4.678400	0.402700	-1.273900
C	-2.632200	-0.562400	0.599700	F	-2.212900	2.400800	-2.195000
F	0.333700	0.495300	1.974500	C	-3.464900	1.421800	-0.462100
C	2.348700	1.440400	1.289800	F	-4.678400	0.402700	1.273900
F	2.800800	-1.506800	-1.522600	F	4.390300	2.360400	0.580100
C	3.611500	0.416700	-0.485700	F	-4.390300	2.360400	-0.580100
F	-0.333700	0.495400	-1.974400				

Table S4. Cartesian coordinates of the optimized structure of $[Mes_2TeMe]^+$ ($[\mathbf{2}]^+$) using M062X functional

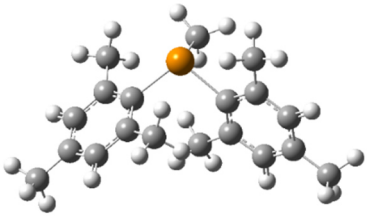

Te	0.034200	-1.439000	-0.313600
C	1.607200	-0.073200	0.048600
C	2.631200	1.753100	1.203100
H	2.577100	2.549900	1.943300
C	1.504300	0.953200	1.007500
C	-1.650500	0.925500	-1.092600
C	2.779300	-0.291500	-0.697900
C	-1.672100	-0.186600	-0.229600
C	-3.840900	0.420100	0.575300
H	-4.704000	0.207800	1.203300
C	3.816800	1.570100	0.489600
C	3.869200	0.544900	-0.453600
H	4.787200	0.384500	-1.015300
C	-0.512300	1.239900	-2.035800
H	0.333000	1.705500	-1.515100
H	-0.850800	1.932500	-2.810700
H	-0.133400	0.348100	-2.555000
C	0.260100	1.284100	1.798000
H	-0.437600	1.884700	1.200800
H	0.528000	1.866400	2.683500
H	-0.293300	0.403300	2.137300
C	-3.842000	1.564800	-0.220300
C	-2.746800	1.786700	-1.057200
H	-2.747100	2.654700	-1.714600
C	-2.774600	-0.481200	0.585000
C	4.998300	2.471600	0.726400
H	4.840000	3.444300	0.245600
H	5.917700	2.042400	0.319200
H	5.145800	2.654900	1.795500
C	0.228800	-2.384500	1.586100
H	0.081100	-1.668100	2.393500
H	1.263100	-2.738700	1.587100
H	-0.461000	-3.224700	1.661200
C	-4.999000	2.527600	-0.208300
H	-5.795500	2.189200	0.459600
H	-5.420100	2.642400	-1.213100
H	-4.673000	3.519500	0.124600
C	-2.880000	-1.716000	1.445600
H	-2.595100	-2.623700	0.898600
H	-3.912500	-1.856500	1.775200
H	-2.260700	-1.646400	2.347600
C	2.914800	-1.382000	-1.737000
H	2.801500	-2.384700	-1.305100
H	3.903900	-1.342500	-2.199800
H	2.174500	-1.278600	-2.540300

Table S5. Cartesian coordinates of the optimized structure of $[Mes(C_6F_5)TeMe]^+$ ([**3**]$^+$) using M062X functional.

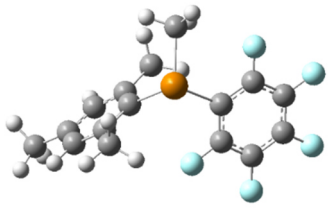

Te	6.543282	6.227819	6.124935	H	5.980052	3.311023	5.371971
F	7.080687	9.446826	6.079400	C	5.602450	2.814056	8.559581
F	5.586642	11.515927	6.953887	H	5.122935	1.856504	8.367972
F	3.730559	6.448398	7.487631	C	6.045385	3.109458	9.848908
F	3.173122	11.058027	8.093578	C	7.490026	6.600892	9.418334
F	2.243386	8.528945	8.362796	H	8.554556	6.583414	9.155522
C	6.368655	4.944305	7.781474	H	7.430267	6.773677	10.495861
C	5.460078	7.898524	6.817076	H	7.025892	7.463436	8.926734
C	6.819177	5.294950	9.069304	C	6.639331	4.352487	10.079951
C	5.742802	3.713364	7.503127	H	6.974980	4.599758	11.085674
C	5.906346	9.206619	6.662381	C	4.204773	7.687219	7.379933
C	8.529551	6.955419	6.340488	C	5.145078	10.282837	7.097521
H	8.584377	7.698617	7.133090	C	3.425626	8.746465	7.823090
H	8.818560	7.386961	5.380931	C	5.896333	2.118287	10.970301
H	9.141355	6.080062	6.573753	H	5.236978	1.292437	10.691303
C	5.200712	3.333667	6.143650	H	5.491315	2.598680	11.866951
H	4.411042	4.020864	5.813660	H	6.872843	1.696798	11.237228
H	4.759816	2.334740	6.180867	C	3.902896	10.047223	7.681931

Table S6. Cartesian coordinates of the optimized structure of $[(C_6F_5)_2TeMe]^+$ ([**4**]$^+$) using M062X functional.

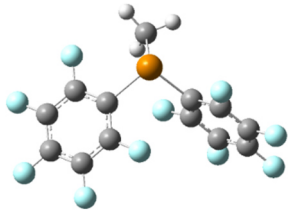

Te	5.536689	4.594558	10.001288	C	2.955736	7.645481	7.190908
F	4.627521	4.451761	6.967670	C	8.715684	4.901318	7.017338
F	2.260852	8.458351	6.433977	C	6.602224	6.014006	11.172321
F	4.139398	7.414652	10.595490	H	6.816091	6.890491	10.560196
F	7.473262	6.479287	8.223124	H	7.519774	5.509339	11.485648
F	3.208716	6.142251	5.402296	H	5.980751	6.265558	12.032983
F	9.906752	3.271471	5.838288	C	7.749029	5.203360	7.963196
F	9.364476	5.859979	6.391393	C	4.175020	5.597904	7.470762
F	8.587867	1.282430	7.110887	C	3.194553	7.976894	8.523694
F	6.692739	1.890288	8.948915	C	7.061261	4.192057	8.631463
F	2.719764	9.097404	9.023131	C	8.995135	3.564169	6.731836
C	4.443773	5.923296	8.797443	C	8.315828	2.538938	7.386874
C	3.444167	6.453175	6.658794	C	7.349954	2.863230	8.329766
C	3.931062	7.108020	9.315923				

Table S7 LUMO and LUMO+1 orbital energies of the telluronium cations and their nuetral precursor in the gas-phase and water phase with SMD solvation model.

Compounds	Gas phase		Water phase	
	LUMO Energy / eV	LUMO+1 Energy / eV	LUMO Energy / eV	LUMO+1 Energy / eV
Mes_2Te	0.41	0.47	0.45	0.46
$Mes(C_6F_5)Te$ (**1**)	-0.47	-0.32	-0.12	-0.04
$(C_6F_5)_2Te$	-1.17	-0.99	-0.44	-0.42
$[Mes_2TeMe]^+$ ($[\mathbf{2}]^+$)	-3.78	-3.53	0.45	0.46
$[Mes(C_6F_5)TeMe]^+$ ($[\mathbf{3}]^+$)	-4.79	-4.18	-0.78	-0.50
$[(C_6F_5)_2Te]^+$ ($[\mathbf{4}]^+$)	-5.54	-5.29	-1.17	-0.89

References

1. C. P. Rosenau, B. J. Jelier, A. D. Gossert and A. Togni, *Angew. Chem. Int. Ed. Engl.*, 2018, **57**, 9528-9533.
2. P. A. W. Dean, V. Manivannan and J. J. Vittal, *Inorg. Chem.*, 1989, **28**, 2360-2368.
3. M. Oba, Y. Okada, M. Endo, K. Tanaka, K. Nishiyama, S. Shimada and W. Ando, *Inorg Chem*, 2010, **49**, 10680-10686.
4. F. Yu, P. Li, B. Wang and K. Han, *J. Am. Chem. Soc.*, 2013, **135**, 7674-7680.
5. T. M. Klapotke, B. Krumm, P. Mayer, K. Polborn and O. P. Ruscitti, *Inorg. Chem.*, 2001, **40**, 5169-5176.
6. A. Kozma, J. Petuskova, C. W. Lehmann and M. Alcarazo, *Chem Commun (Camb)*, 2013, **49**, 4145-4147.
7. H. J. Clarke, E. N. Howe, X. Wu, F. Sommer, M. Yano, M. E. Light, S. Kubik and P. A. Gale, *J. Am. Chem. Soc.*, 2016, **138**, 16515-16522.
8. A. V. Jentzsch, D. Emery, J. Mareda, S. K. Nayak, P. Metrangolo, G. Resnati, N. Sakai and S. Matile, *Nat. Comm.*, 2012, **3**, 905.
9. L. M. Lee, M. Tsemperouli, A. I. Poblador-Bahamonde, S. Benz, N. Sakai, K. Sugihara and S. Matile, *J. Am. Chem. Soc.*, 2019, **141**, 810-814.
10. G. M. Sheldrick, *SADABS, Version 2007/4, Bruker Analytical X-ray Systems, Inc., Madison, Wisconsin, USA*, 2007.
11. G. M. Sheldrick, *Journal*, 2000.
12. O. V. Dolomanov, L. J. Bourhis, R. J. Gildea, J. A. K. Howard and H. Puschmann, *J. Appl. Crystallogr.*, 2009, **42**, 339-341.
13. M. J. Frisch, G. W. Trucks, H. B. Schlegel, G. E. Scuseria, M. A. Robb, J. R. Cheeseman, G. Scalmani, V. Barone, G. A. Petersson, H. Nakatsuji, X. Li, M. Caricato, A. V. Marenich, J. Bloino, B. G. Janesko, R. Gomperts, B. Mennucci, H. P. Hratchian, J. V. Ortiz, A. F. Izmaylov, J. L. Sonnenberg, Williams, F. Ding, F. Lipparini, F. Egidi, J. Goings, B. Peng, A. Petrone, T. Henderson, D. Ranasinghe, V. G. Zakrzewski, J. Gao, N. Rega, G. Zheng, W. Liang, M. Hada, M. Ehara, K. Toyota, R. Fukuda, J. Hasegawa, M. Ishida, T. Nakajima, Y. Honda, O. Kitao, H. Nakai, T. Vreven, K. Throssell, J. A. Montgomery Jr., J. E. Peralta, F. Ogliaro, M. J. Bearpark, J. J. Heyd, E. N. Brothers, K. N. Kudin, V. N. Staroverov, T. A. Keith, R. Kobayashi, J. Normand, K. Raghavachari, A. P. Rendell, J. C. Burant, S. S. Iyengar, J. Tomasi, M. Cossi, J. M. Millam, M. Klene, C. Adamo, R. Cammi, J. W. Ochterski, R. L. Martin, K. Morokuma, O. Farkas, J. B. Foresman and D. J. Fox, *Journal*, 2016.
14. Y. Zhao and D. Truhlar, *Theor. Chem. Acc.*, 2008, **120**, 215-241.
15. K. A. Peterson, D. Figgen, E. Goll, H. Stoll and M. Dolg, *J. Chem. Phys.*, 2003, **119**, 11113-11123.
16. T. Lu and F. Chen, *J. Comput. Chem.*, 2012, **33**, 580-592.